INVESTIGATION OF ASPHALT BINDERS BY X-RAY DIFFRACTION USING PEARSON–VII, PSEUDO–VOIGT AND GENERALIZED FERMI FUNCTIONS

KASSU GEBRESELLASIE

INVESTIGATION OF ASPHALT BINDERS BY X-RAY DIFFRACTION USING PEARSON-VII, PSEUDO-VOIGT AND GENERALIZED FERMI FUNCTIONS

by

© Kassu Gebresellasie
B.Sc. (Physics and Applied Mathematics)

A thesis submitted to the
School of Graduate Studies
in partial fulfillment of the
requirements for the degree of
Master of Science.

Department of Physics & Physical Oceanography
Memorial University of Newfoundland

August 14, 2012

Contents

Abstract

Asphalt binder of twenty-three samples were obtained from Alberta, Northern Ontario, Canada, Montana USA, and Venezuela. Thin films samples (1mm) were prepared by heating onto glass slides at 150°C for 10 min. X-ray diffraction (XRD) patterns were obtained using monochromatic Cu-K-α radiation at 40kV and 40mA on Rigaku DMax 2200V-PC. Profile fitting was performed using Pearson VII and Pseudo-Voigt functions over 5° to 35° and 60° to 110°$= 2\theta$. Furthermore, to our knowledge, it is the first time we introduced XRD spectra modeled using a Generalized Fermi Function (GFF) for asphalt binders. The analysis of the diffraction line broadening in x-ray thin film is analytically calculated and simulated using these functions. The results showed a correlation among Pearson VII, Pseudo-Voigt and GFF.

X-ray line broadening investigations from the integral width or the full width at half maximum (FWHM) of the diffraction line is used for approximation of the experimental x-ray line profiles obtained from the samples. Asphalt binder samples measured by x-ray diffraction on thin asphalt films, are identified as two factors that correlate reasonably well with aging tendency at low temperatures. From the application perspective, cracking in asphalt pavements in colder climates and rutting in hot climates are on-going problems. Therefore, investigation and understanding of structural and compositional properties of asphalt binders at the microscopic level is aimed at improving the performance and durability of asphalt pavements.

Acknowledgements

Primarily, I would like to sincerely thank my supervisors Dr. John Shirokoff and Dr. John Lewis for their encouragement, guidance, and most importantly, their friendship during my graduate studies at Memorial University. Their mentorship was of greatest importance in providing me a well rounded experience consistent with my long-term career goals. They encouraged me to not only grow as an experimentalist and applied physcist but also as an independent thinker. For everything you have done for me, Dr. John Shirokoff and Dr. John Lewis, I thank you. Additionally, my gratitude goes to the Department of Physics and Physical Oceanography faculty and stuff for their professional and freindly support whenever I need, valuable discussions and accessibility. In particular, I would like to thank Dr. Todd Andrews, expertise and patience. Finally, and most importantly, I would like to thank my mother Birke Mamo for her prayer support, encouragement, and unwavering love were undeniably the bedrock upon which my life have been built. I thank my friends Nunu, Feven, and Yohannes , I can not even dream to reach here without your assistance during the make or break time, I salute and thank all of you from the bottom of my heart. Also, I thank Wegayehu and Bethelhem, for their enocouragment and support. It was under their watchful eye that I gained so much drive and an ability to tackle challenges head on.

"Egze-abher Yistelegn. Amesegnalehu."

List of Tables

List of Figures

Abbreviations

P	Pearson VII
V	Pseudo-Voigt
FWHM	Full width at half maximum of profile
HMA	Hot Mix Asphalt
WMA	Warm Mix Asphalt
CMA	Cold Mix Asphalt
PAV	Pressure Aging Vessel
SHRP	Strategic Highway Research Program
GFF	Generalized Fermi Function
SARA	Saturates, Aromatics, Resins and Asphaltenes
DSR	Dynamic Shear Rheometer
BBR	Bending Beam Rheometer
PG	Performance Grade
ASTM	American Society for Testing and Materials
AASHTO	American Association of State Highway and Transportation
DTT	Direct Tension Test
SMA	Specially Modified Asphalt
CGSB	Canadian General Standards Board
TFOT	Thin Film Oven Test

XRD   X-ray diffraction

XPS   X-ray Photoelectrics Spectroscopy

Specimen ID	XRD Filename
L1	RR1Lage1W
L2	RR2Lage1W
L3	RR3Lage1W
L4	RR4Lage1W
L5	RR5Lage1W
L6	RR6Lage1W
L7	RR7Lage1W
N1	HWY11 − 5102age1W
N2	HWY11 − 5106age1W
N3	HWY11 − 5108age1W
E9	E009age1W
AAE	AAEage1W
O1	SC58 − 34age1W
O2	PC58 − 34age1W
H1	HearstAage1W
H2	HearstBage1W
T1	655−1age1W
T2	655 − 2age1W
T3	655 − 3age1W
T4	655 − 4age1W
T5	655 − 5age1W
T6	655 − 6age1W
T7	655 − 7age1W

Symbols

*	Convolution
γ	γ band (peak) on XRD pattern
$(002)_{graphane}$	$(002)_{graphane}$ band (peak) on XRD pattern
(10)	(100) band (peak) on XRD pattern
(11)	(110) band (peak) on XRD pattern

Chapter 1

Introduction

1.1 Asphalt and Asphaltene

Asphalt is a mixture of aggregates, binder and filler, used for constructing and maintaining all kinds of roads, air ports, parking areas, etc. Typical asphalt mixtures are aggregates of crushed rock, sand and gravel. To achieve, a good cohesive mixture of the aggregates, we use a binder to hold them together. Particularly, bitumen is widely used as a binder for binding aggregates. Asphalt pavement consists of the road structure above the subgrade which includes unmixed and bituminous mixed materials. This gives the pavement the ability to distribute the loads of the traffic before it breaches at the subgrade or as sometimes called formation level.

Furthermore, asphalt is highly viscous liquid that is available in most crude petroleum and in some natural deposits such as natural asphalt in Trinidad lake. Asphalt has been the primary choice in roads and similar pavement constructions due to its excellent candidacy for pavement. Asphalt is a pavements major factor that leads to its deterioration (aging), due to its sensitivity and easily oxidized. Therefore, it is very important to study and investigate vigorously the performance of asphalt

1
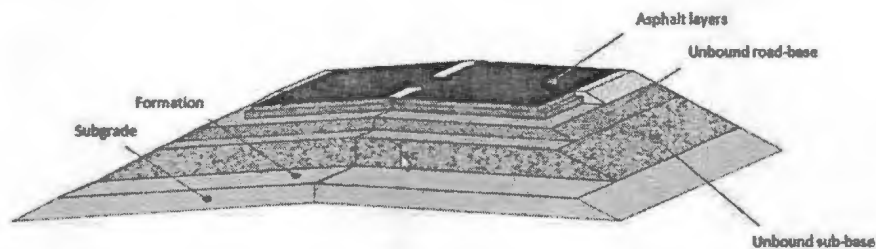
Figure 1.1: Schematic layers of pavements (www.eapa.org).

pavement at the microscopic level, such as structure, properties so that in improving durability.

Asphaltenes are high molar mass brown to black solids and consist of a complex mixture of heavy crude constituents. By definition, they are soluble in aromatic solvents (benzene or toluene) and insoluble in paraffinic solvents (n-pentane or n-heptane).

Asphaltene deposits can be extracted during petroleum production, transportation, and upgrading processes due to changes in temperature, pressure, and composition. Many scholars proposed methods that can be applied to investigate, conduct an experiment and analyze the aging of organic compounds, especially, the most mysterious part of bitumen component, asphaltene, using such as XRD analysis, NMR, etc. One of the pioneered and most significant studies in asphaltene is done by Yen et al. (1961) who used x-ray analysis of asphaltenes to determine structure and intensive review is followed in section 2.1.

1.1.1 Properties of Asphaltene

Speight (1999) defined asphaltenes as the fraction separated from crude oil or petroleum products upon addition of hydrocarbon solvents such as n-heptane. An elemental

Source	Composition(wt Perc.)					Atomic Ratios			
	C	H	N	O	S	H /C	N/C	O/C	S/C
Canada	79.0	8.0	1.0	3.9	8.1	1 .21	0.011	0.037	0.038
Iran	83.7	7.8	1.7	1.0	5.8	1 .19	0.017	0.009	0.026
Iraq	80.6	7.7	0.8	0.3	9.7	1 .15	0.009	0.003	0.045
Kuwait	82.2	8.0	1.7	0.6	7.6	1 .17	0.017	0.005	0.035
Mexico	81.4	8.0	0.6	1.7	8.3	1 .18	0.006	0.016	0.038
Sicily	81.7	8.8	1.5	1.8	6.3	1 .29	0.016	0.017	0.029
USA	84.5	7.4	0.8	1.7	5.6	1 .05	0.008	0.015	0.025
Venezuela	84.2	7.9	2.0	1.6	4.5	1 .13	0.020	0.014	0.020

Table 1.1: Elemental Composition of Asphaltene from World Sources (Speight, 1999).

composition of asphaltene is given in Table 1.1.

On the other hand, resins are defined as the fraction of the non-asphalt oil that is strongly present in materials such as silica, alumina, and can only be removed by a solvent such as a mixture of toluene and methanol. Since asphaltenes are aromatic heterocompounds with aliphatic substitutions and as a result, they form the most polar portion of crude oil. Furthermore, Koots et al. (1975), suggested that resins have reasonable correlation with asphaltenes and concluded that this affiliation determines solubility in crude oil. An example of a proposed molecular structure of asphaltene is seen in Figure 1.2.

1.1.1.1   Physical Properties and Characteristics of Asphaltenes

The study of asphaltenes and resins has been the interest of researchers since 1930s, when it was realized that asphaltenes can easly be found throughout nature. As-
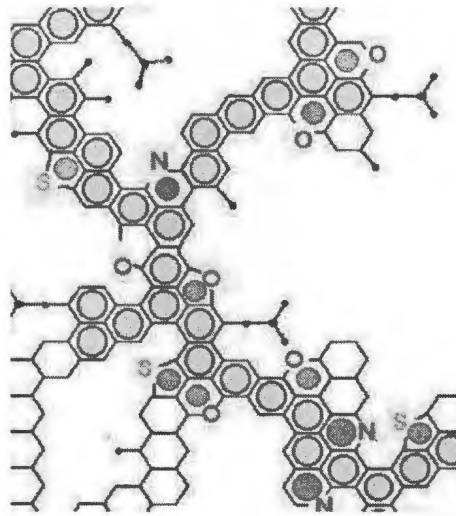
Figure 1.2: Modified molecular structure of asphaltene (Figure altered from Altamirano et al., 1986).

phaltenes can be found from a variety of forms such as, bitumen and in dispersed organic matters in sediments. The definition of asphaltene in general described as, the fraction of heavy organics from carbonaceous sources such as petroleum, coal, and shale oil that is insoluble in low molecular weight n-paraffins and soluble in aromatic solvents such as benzene and toluene (Mansoori et al., 1988). At present, many scholars agree to the definition of asphaltenes as an operational material entirely based on solubility as shown in the figure 1.3. Mullins (2010), principally bases his defination of asphaltene on the molecular weight analysis by showing different hierarchial stages using the Yen-Mullins model.

The solubility curves in figure 1.3 below indicate that the soluble fraction cooperatively undergo via solivation and form the precipitate fraction when they interact in solution. The precipitate solubility curves provides the most convincing support for cooperative aggregate interaction because the precipitate asphaltenes become insoluble at a much higher toluene fraction than the whole asphaltenes. If the precipitate
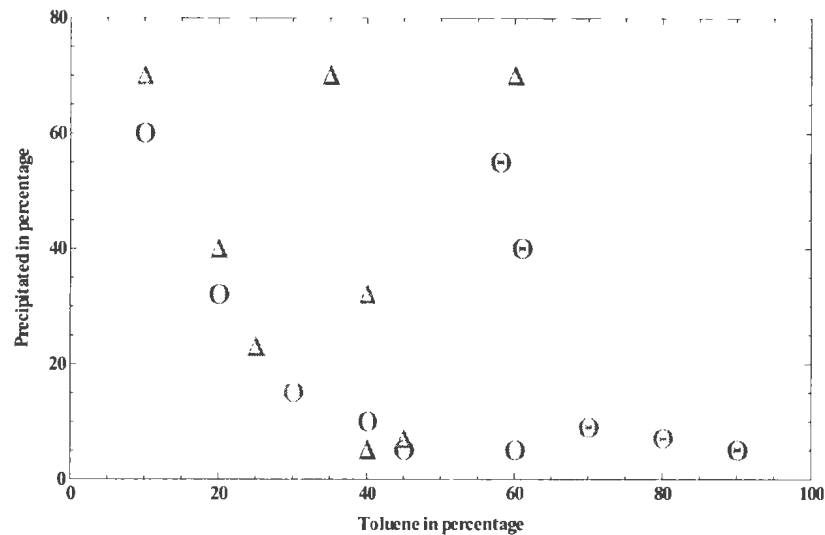
Figure 1.3: Modified figure of solubility, where delta indicates solubility with Resins; theta symbolizes precipitate and O represents whole with Resins (Keith, 2003).

fraction asphaltenes were appreciably non-interacting, they would begin to precipitate at the same heptol ratio as the whole and then proceed at a much steeper slope. In 2003, Keith et al., showed that the soluble fraction was far more soluble than either the whole or precipitate.

However, the true structural definition of asphaltene may never be quantized due to an enormous varities of molecules in crude oil. Most researchers agree that asphaltenes contain polynuclear aromatics, aliphatics, and alicyclic moieties with small amounts of dispersed heteroelements such as oxygen, sulfur, vanadium, and nitrogen. In addition, in terms of molecular weight and aromaticity, asphaltenes are the heaviest fraction of a distribution of compounds that include aromatics and resins. Recently, however, Mullins (2011) showed the most up to date definition of asphaltene using a variety of methods to create the modified Yen model.

In this research, we investigate asphalt binders collected from different parts of

Canada. The asphalt binders are aged for a week and the x-ray diffraction profiles are collected and analyzed accordingly from the Rigaku diffractometer, by the aid of advanced mathematical functions of Pearson-VII and Pseudo-Voigt and Generalized Fermi Function (GFF).

1.1.2   Types of Asphalt

Providing the best performance to different construction designs, one can use various proportions of asphalt mixture. Due to the different requirements, for exapmle, a road construction needs to consider high traffic load, extreme hot or extreme cold weather conditions. Thus, the mix used has to have the capacity to withstand stiffness and deformation. However, the need to have sufficent flexibility and strength to resist cracking caused by different pressures exerted on the road is essential for reasonable durability of the pavement. A good knowledge of the catagories of asphalts during mixing is important for achieving proper standard in performance and durability. Thus, some of the major types of asphalt are listed below:

a) Hot Mixe Asphalt (HMA), commonly are produced at temperatures range from 150° C - 190° C. But, depending on the intended use, a different asphalt mixture can be used.

b) Warm Mix Asphalt (WMA), is however produced at temperature range of 20° C-40° C, which is much lower than the HMA. The advantage of producing WMA is, that it utilizes less energy. The two important points to note during WMA are: having sufficient stiffness and resistance to deformation in order to cope with the applied pressure due to heavy trucks for example. Furthermore, the need to have an adequate flexural strength to resist cracking.

c) Cold mix are produced without heating the aggregate. This is only possible, due

to the use of a specific bitumen which breaks either during compaction or during mixing. After breaking, the emulsion coats the aggregate and over time, increases its strengths. Cold mixes are particularly recommended for lightly trafficked roads, in rural areas.

Asphalt can be broadly classified into two categories. Natural asphalts are deposited in layers for thousands of years whereas, the petroleum asphalts are colloidally dispersed hydrocarbons residue from crude petroleum distillation during refinary process. Today asphalt from petroleum crude is mostly used for pavments. Rigid pavements are constructed using Portland cement concrete while flexible pavements are constructed using asphalt. Flexible pavement failure can be attributed to causes such as changes in the crude source and refining processes; improper mix design; increased truck traffic volume; tire pressure and axle loading; deficiency in specifications and improper use of additives. Improper mix design, improper use of aggregates in asphalt binders, asphalt pavement failures and the XRD analysis method will be discussed in the literature review section.

1.1.2.1   Natural Asphalt

Natural asphalt, such as (Trinidad lake asphalt), is an organic compound that reacts with oxygen, and hence changes the structure and composition of its asphalt molecules. As a result, the asphalt loses its sticking ability. Relatively, oxidation tends to occur more rapidly at high temperature than at low temperature. Natural asphalts are mostly used to replace some of the bitumen content in an asphalt mix and improve the overall surface performance and deformation resistance.

1.1.2.2   Petroleum Asphaltene

Petroleum asphaltene represents a class of petroleum liquids. It is the most refractory and often the heaviest oil component (Sheu, 2002). Such properties associated with asphaltene may include molecular weight and structures. It has taken researchers over a century trying to understand asphaltene molecular and colloidal properties. Yet, many issues around asphaltene are controversial until recently (Mullins, 2010) showed elegantly that at least the first attempt to have the best approximation of asphaltene's molecular weight.

As briefly discussed in the literature review, asphaltene was identified by Boussingault in 1937 from an ether insoluble fraction of asphalt. In 1933, Nellensteyn suggested that asphaltenes are high molecular hydrocarbons forming a colloidal system adsorbed by lighter components on the surface. However, his proposal was directed to studying fundamental properties of asphaltene molecules, such as molecular weight, structure, etc. During the early 1900's, many scholars believed that asphaltene molecular properties might not be as important as it was believed by others and supportive of the concept proposed by the asphaltene discoverer (Boussingault, 1937). However, active research has been taking in understanding the structure, molecular weight and other properties of asphaltene is the crucial concept for many applications and production efficency of petrolum products.

1.1.2.3   Asphalt Cement

Asphalt cement is composed of bitumen, resins, absorbed gas, etc., and distillation process can occur either naturally, resulting in asphalt lakes (Trinidad asphalt), or it can be performed through the petroleum refining process. The crude source type and the distillation process determines the proportion and content of these compounds in

asphalt cement. Asphalt cement goes under chemical and physical changes, due to the raction of the ingredients with it through time. In general, as the asphalt cement ages, it becomes stiffer (Richard, 2007). In the refining process, the heavy residue from this stage of refining is further processed to produce various grades of asphalt cement. Asphalt cement, now called Performance Grade (PG) binders, is selected on the basis of climate and traffic at the location where it is intended be used.

1.1.3 Performance Grade (PG)

Performance grade (PG) or (binder grading) system, includes specifications that relate measured physical properties of asphalt binders to field performance. Performance grading tests use aging conditions, temperatures, and loads that are similar to those encountered in the pavements of interest. For example, PG binder designation of PG 67-31 would be read as; the first number, 67, is the high temperature in degrees Celsius that the pavement is expected to reach. The second number, 31, is the lowest temperature that the pavement perform well in the standard. PG 67-31 asphalt is soft enough to resist low temperature thermal cracking down to a temperature of 31°C, as a result it prevents a pavement from rutting in hot seasons when pavement temperatures become as high as 67°C.

PG binder specifications require that the asphalt to be modified with polymers or other chemicals to enhance its properties and meet performance requirements. Adding these modifiers however have negative consequences, i.e., by reducing the temperature susceptibility and age hardening. On the other hand, the advantage of these type of binders is that, they resist low temperature cracking, and improve stiffness of the asphalt at high temperatures, hence, reducing rutting. However, the economic aspect of modified asphalts is far reaching since it can cost nearly twice as much as unmodified

asphalts (Hesp, 2008). By weight, asphalt generally accounts for between four and eight percent of the hot mix asphalt (HMA) and makes up about 25 to 30 percent of the cost of an HMA pavement (Monismith, 1985).

1.1.4 Asphalt Binders and Asphaltene

Asphalt binders refer to the binding agent that glues the aggregate together in a hot mix asphalt (HMA). Asphaltene is a molecular compound that has a high resistance to cracking and hence decreases petrolum production during distillation. However, the presence of high proportion of asphaltene is the best candidate for making highway surfaces. Many of the properties that make asphaltene useful thus depend on the application in question. For example, asphalt with higher percentage of asphaltene is the best choice for highway surface applications. This research work also discloses the impact of mix and improper mix on the performance of pavements, such as in North Ontario and Alberta, where the asphalt binders samples obtained and analyzed are with different techniques.

1.1.5 Rutting and Cracking

Two of the main phenomenon that affect asphalt pavements performance are rutting and fatigue. Rutting is characterized by permanent deformation of the pavement. It generally develops during the hot seasons, when the asphalt is soft, while fatigue cracking is characterized and occurs during cold to mild seasons. The first phase of fatigue is identified with longitudinal cracks, and followed by alligator cracking in an advanced damage stage to the pavement. We believe that, for improving the rutting and fatigue performance of an asphalt pavements, extensive studies of the structural and compositional characterstics of asphalt binder at its microscopic level is crucial.

1.1.5.1   Rutting

Highway rutting is common due to higher repetition of traffic. For instance, rutting is less on airport pavements due to lower aircraft traffic and more room for taking off and touching down. However, there are still some factors contributing to rutting, such as high pressure from plane tires, of course the most important part is, proper pavement mix content and the weather conditions in the location. Surface rutting can also occur when one or more of the HMA layers fails and is usually accompanied by depressions in the surface, while subgrade rutting occurs when the subgrade is unable to support the loads to which it is exposed as we observe from the illustration below in figures 1.4 and 1.5.
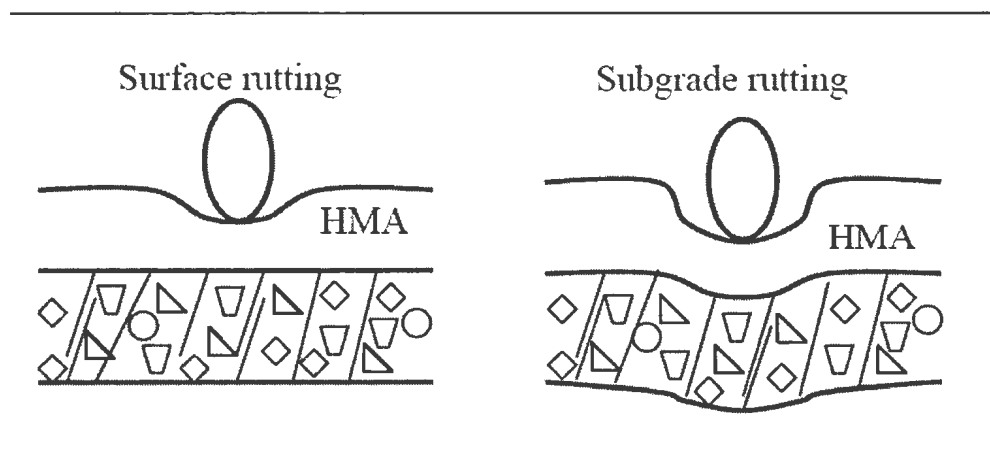
Figure 1.4: Sketch of surface cross-section and subgrade rutting.

Pavement settles into the subgrade causing surface depressions in the wheel path. Considerable research has been conducted to set a limit on binder and aggregate influence on rutting potential that must be sufficiently strong to resist excessive shear loads generated between the aggregate particles at higher temperatures.

Many scholars, investigated some of the potential causes of rutting. McGennis

Figure 1.5: Rutted road surface due to too soft asphalt binders being used.

and co-workers (1994), reported impurities in binder, such as, percent of mineral filler, and thickness of film are among hot mix asphalt mixture properties found to affect mixture rutting performance. In 2002, Christensen and Bonaquist, found out that from civil engineering perspective, HMA mixture shear strength increases as asphalt binder gets stiffer.

1.1.5.2   Fatigue Cracking

Persistent bending due to traffic loading over time on asphalt pavements is the measure cause of fatigue cracking (see figure 1.6). Through time, the deterioration on internal structure increases, which means the stiffness, degradation of the load carrying capacity and ability to resist further damage of the HMA pavement decreases.

They sometimes are known as alligator cracks and can be recognized by the pattern of interconnected chaotic cracks in the pavement surface. Galal and White,

Figure 1.6: Fatigue cracked road surface due to too hard asphalt binders being used.

(2001) reported that low temperatures are responsible for fatigue cracking and can be accelerated by pavement aging. Hence, the major possible causes of fatigue cracking can be increased loading, inadequate structural design, and the most crucial of all is mixture composition.

Harvey and co-workers (1995) found out, more asphalt binder availability and less air void content may result in the increased fatigue life of HMA mixtures. On the other hand, the more binder content in the hot mix, the higher binder film thickness and hence, less strains and less stress in the binder. However, decreasing the air void content shows stiffness and strength of HMA increase, the stress level in both the aggregate and binder decrease.

Lower air void content also makes for a more smooth binder aggregate structure resulting in less stress concentration at critical solid air interfaces. In mixtures with

the combination of high binder content and low air void content, providing longer fatigue life. In 1995, Monismith, investigated correlation among HMA mixtures that are stiff and pure asphalt binders, result in failure in the fatigue life of mixtures.

1.2   X-ray Diffraction (XRD) Measurements

X-rays primarily interact with electrons in atoms. When x-ray photons collide with electrons, some photons from the incident beam will be deflected away from the direction where they originally travel. If the wavelength of these scattered x-rays did not change i.e, x-ray photons did not lose any $h\nu$ of energy, the process is called elastic scattering (Thompson Scattering) where only momentum has been transferred during the scattering process. These are the x-rays that we measure in diffraction experiments, as the scattered x-rays carry information about the electron distribution in the thin film of the specimen (asphalt binders).

On the other hand, in the inelastic scattering process (Compton Scattering), x-rays transfer some of their energy to the electrons and the scattered x-rays have different wavelength (λ) than the incident x-rays. Diffracted waves from different atoms can interfere with each other and the resultant intensity distribution is strongly modulated by this interaction.

1.2.1   X-Ray Scattering Theory

Highly collimated beam, combined with a long distance between the sample and the detector, allow sensitive measurements of the x-rays that are just barely scattered by the sample (scattering angle $< 6°$). From Bragg's Law, the length d is inversely proportional to the scattering angle, therefore, small angles represented larger features in the samples (see section 2.1.1).

Our analysis of the collected data of asphalt binders is based on the assumption of Yen model, i.e, atoms are rearranged themselves in a periodic fashion and a simple cubic structure with four known peaks. In addition, we discuss the new Yen-Mullins model in relation to the XRD analysis in section 2.1.2.

1.3   Objectives of The Research

The objective of this research is to investigate XRD analysis on asphalt structure, properties and performance. Furthermore, this work is intended to develop the main pavement deterioration model for asphalt pavements focusing on at the molecular level of asphalt binders. A total of twenty three different samples of asphalt binders, are taken from diffferent parts of Canada and tested in the laboratory for aging and investigating the composition of the aggregates at the microscopc level.

The aging asphalt specimens are simulated using three of the major mathematical functions (Pseudo-Voigt, Pearsen VII, and Generalized Fermi Function). This is just a simulation based on real aging asphalts from the specimen. The XRD profiles were performed and the results analyzed. The XRD data show it is possible to differentiate asphalts of different standards and classifications through peak centroid and other parameters (such as aromaticity and crystallite) are considered.

Chapter 2

Literature Review

2.1 Asphaltene Structure and X-Ray Diffraction

One of the pioneered and most significant studies in asphaltene is done by Yen et al. (1961), who used x-ray analysis of asphaltenes to determine structure of asphaltene. In the same year, Yen and his co-workers investigated asphaltenes using x-ray diffraction and they concluded that according to their measurements, asphaltene is composed of a stack of clusters of n-alkyls. Large margin of error of the x-ray diffraction signal collected to the aromatic clusters and causes a great deal of uncertainities that evolve to the degree of condensation (Dickie et al., 1961).

As a result of this study, however, subsequent study was also concluded by Dickie and Yen (1967). Yen (1974) proposed the first model and it is called the Yen Model, of the asphaltene's structure that postulates simple cubic structure model as a foundation. However, this model has not been accepted by many researchers, but Yen and his collaborators' original idea has continously been receiving attention for the last 40 years. Furthermore, they reported that strong chemical forces are responsible for asphaltene's elements such as carbon, hydrogen, and heteroatoms to keep them

together.

XRD has been widely used to study the macrostructure of asphaltenes (Yen et al., 1961). Sadeghi et al. (1986) reviewed the fundamental principles of the XRD for asphaltenes. Christopher with his colleagues (1996) and Shirokoff et al. (1997) studied asphaltene macrostructure and crystallite parameters by using XRD and NMR methods and showed that there is correlation between the information collected from XRD and NMR. The XRD method is one of the principal techniques that, provides knowledge about the macrostructure and crystallite parameters of the asphaltenes. The description of x-ray results of carbon compounds mainly depend on the experimental results of both aromatic and waxes of hydrocarbons in various concentrations (Sadeghi et al., 1986).

In some of our samples, the result showed that parafinic waxes dominate compared to aromatic hydrocarbones as discussed in chapter 4. Michael et al. (2005) gives a brief description of the aromaticity and crystallite parameters, such as the average distance between the aromatic sheets d_m, the average distance between the aliphatic chains d, the average diameter of the aromatic sheets L_a, the average diameter of the cluster L_c, and the average number of aromatic sheets per cluster M. Siddiqui et al. (2002) investigated crystallite parameters of asphaltenes by catagorizing the samples as fresh and aged Arabian asphalts. The structural transformations of asphaltene molecules in thermal processing of vacuum residue by XRD extensivly studied by (Michael et al., 2005). Furthermore, these researchers, determined the macrostructure and aromaticity parameters using XRD and compared them with the average structural parameters calculated from NMR.

Asphaltenes give non flexibility and strength to bitumen by holding the structure so that it controls various properties of bitumen. The differences in the properties of various bitumens can be described, thus recognizing the structural and functional

characterstic of asphaltenes is essential. Due to dependence of the molecular properties of petroleum and its components on distinct parameters, a lot of rigorous research has been done on the study of basic structural units within bitumen by Yen and Erdman (1963) and later by Strausz et al. (1992). Procedures such as XRD and NMR, and IR spectroscopy have been sucessful in revealing a lot of information about the overall structure of asphaltenes. In this research however, we use XRD as the main tool for investigation of asphaltene and asphalt binders specimen properties. Yen and Erdman (1963) used XRD for structural characterization of asphaltenes and resins in crude oil. Based on the XRD data, these authors proposed a macrostructure for asphaltenes.

Sadeghi et al. (1986) summerized the fundamental theory and application of XRD for asphaltene characterization. Furthermore, based on an XRD study, Dickie and Yen (1961) proposed a macrostructure which represents crystallites and particles of asphaltenes. Schwager et al. (1983) examined the macrostructure and crystallite parameter of different asphaltene samples and used XRD and NMR procedure to estimate the size of the average aromatic structural unit and the number of such units per molecule. Particularly, XRD studies on asphaltenes by Decroocq et al. (1992) revealed structural transformations during heat treatment, which is based on the change in peak position and intensity of the γ and (002) bands. In 1983, Ebert et al. reported XRD of wax (n-paraffins) and stacked aromatic molecules and described the problems of determining the average structure of asphaltenes. Based on the XRD pattern of various paraffins, naphthenes and aromatics, the author and coworkers showed that the γ band originates from paraffinic ordering and that the carbon atoms that are not in stacks do not contribute to (002) band.

As mentioned above, x-ray diffraction is one of the best tool for identification of petroleum asphalt and analysis. The reason being that the peak centroid value
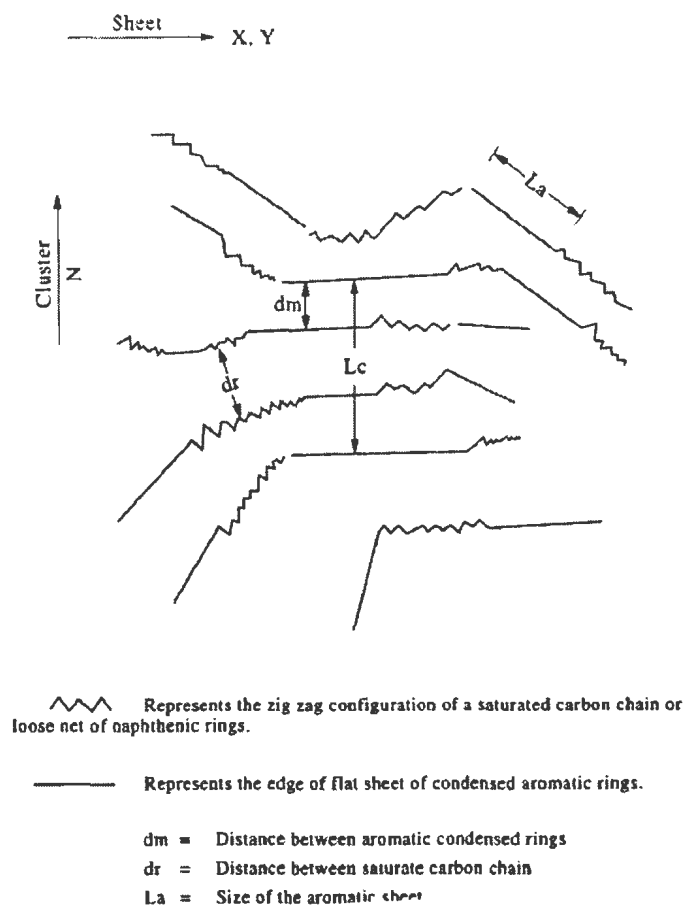
Figure 2.1: Cross-sectional view of asphaltene (Jayaraj et al., 1996).

is the best for asphalt identification and does not changed significantly over time. It is shown that XRD is efficient for asphalt identification, and asphalt crystallinity grows up with the time of weather exposition but not in a direct proportionality form as expected. However, increase of crystallinity can be related with the increase of viscosity characteristics of aging petroleum. As a result, we may expect some x-ray scattering and angles change their position which indicates a possible change of distance between atoms planes given by Bragg's Law as seen in figures 2.1 and 2.2.
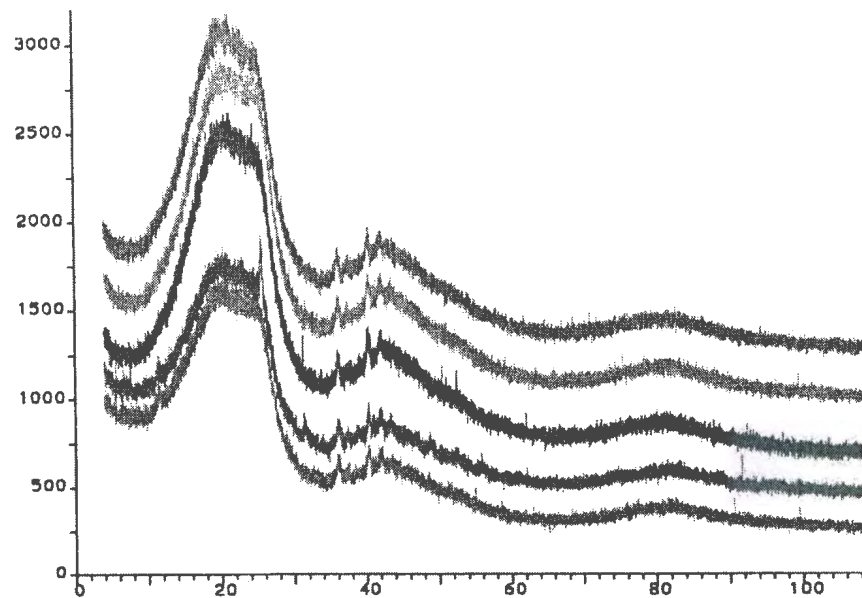
Figure 2.2: Several modified results of asphalt binders peaks as observed from XRD in Counts versus 2θ (Siddiqui et al., 2002).

2.1.1   Role of X-ray Diffraction in Studying Asphaltene Structure

The diffracted waves will consist of sharp interference peaks with the same symmetry as in the distribution of atoms. Measuring diffraction pattern allows us to observe

how distribution of atoms in a material are arranged. Generally, the peaks in x-ray diffraction pattern are directly related to the atomic distances. If one considers an incident x-ray beam interacting with the atoms arranged in a periodic fashion as shown in the 2D figure 2.3.

$$\lambda = EFG = 2\,EF$$
$$EF = d_m \sin\theta$$
$$\lambda = 2\,d_m \sin\theta$$
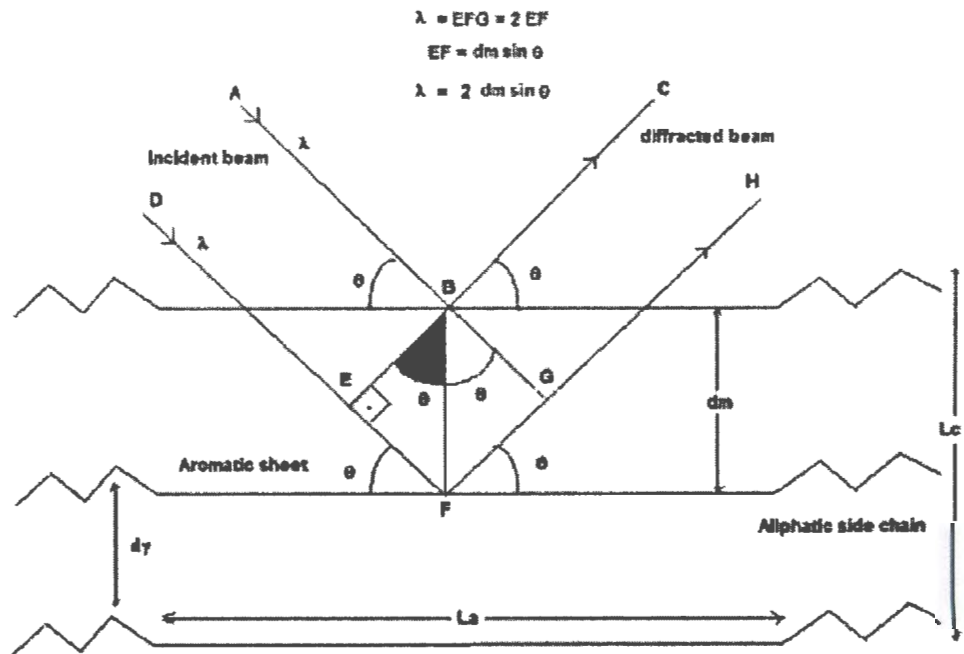
Figure 2.3: Diffraction of x-ray through cross sectional view of asphaltene clusters.

For a given set of lattice planes with an interplane distance of d, the condition for a diffraction peak to occur can be simply written as,

$$2d\sin(\theta) \;=\; n\lambda \qquad\qquad (2.1)$$

which is the famous Bragg's law. In the equation, λ, θ and n are the wavelength of the x-ray, the scattering angle, and an integer representing the order of the diffraction

peak respectively. The Bragg's Law is one of most important laws used for interpreting x-ray diffraction data. It is important to point out that although it is assumed that atoms are scattering points in this example, Bragg's Law applies to scattering centers consisting of any periodic distribution of electron density. The law also holds true if the atoms are replaced by molecules or collections of molecules, such as asphalts in the thin film forms that we used as samples in this study.

XRD is one of the widely used methods for unvailing structural information from asphaltene aggregates, that means, it exposes inner structural information of the cluster of associated asphaltene molecules with stacked aromatic sheets (see Figure 2.4).
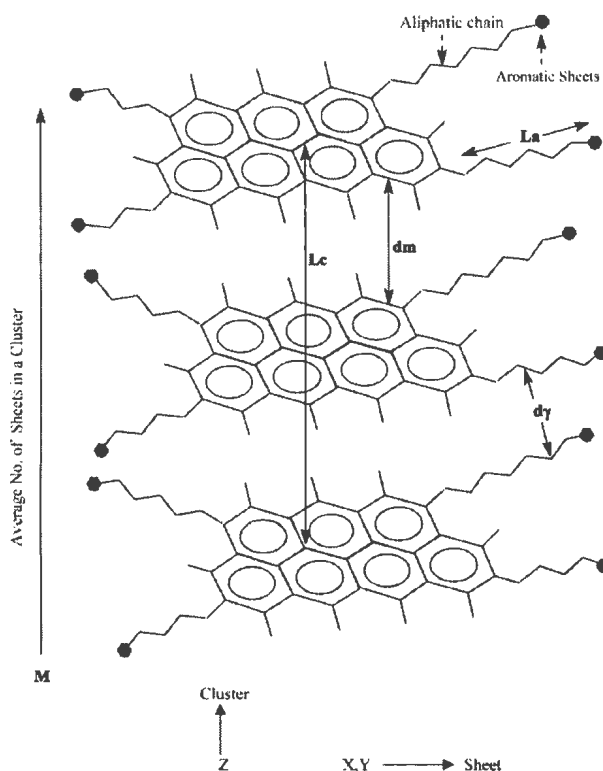
Figure 2.4: Asphaltene cluster showing the main crystalline parameters.

To quantitatively analyze the x-ray diffraction data, the areas under the peaks and the particular distances are calculated, from which the procedure established by (Dickie and Yen, 1982) can be used to determine the aromaticity. Yen defined the aromaticity as,

$$A_r = \frac{C_{ar}}{C_{ar} + C_a} \tag{2.2}$$

$$= \frac{(002)_{area}}{(002)_{area} + \gamma_{area}} \tag{2.3}$$

where C_{ar} is the percentage of aromatic carbons from (002) band and C_a the percentage of aliphatic carbons from γ band. The intersheet distance d_{002} and the interchain distance $d\gamma$ can be calculated from the (002) peak and γ bands, respectively. The Scherrer equation was applied for calculation of the average number of sheets per cluster and the average area of a sheet. The average size of the aromatic clusters perpendicular to the plane of the sheet L_c can be deduced from the (002) band using the Scherrer equation:

$$L_c = \frac{0.9\lambda}{w \cos(\theta)} \tag{2.4}$$

$$= \frac{0.45}{FWHM_{(002)}} \tag{2.5}$$

where, w is the Full Width of the peak at Half Maximum (FWHM). From d_{002} and L_c one can determine the average number of associated sheets in a single micelle:

$$n = \frac{L_c}{d_{(002)}} \tag{2.6}$$

An example of asphalt grade loss due to L_c is shown in Figure 2.5.

Figure 2.5: Modified asphaltene cluster size in the x-ray diffraction spectrum due to worst 3-day grade loss (Hesp et al., 2007).

The average diameter of an aromatic sheet L_a is calculated from the (100) or the (110) peak as,

$$L_a = \frac{1.84\lambda}{(w\cos(\theta))} \tag{2.7}$$

$$= \frac{0.92}{FWHM_{(110)}}. \tag{2.8}$$

An example of asphalt grade loss due to L_a is shown in Figure 2.6.

Figure 2.6: Modified asphaltene sheet size in the x-ray diffraction spectrum during worst 3-day grade loss (Hesp et al., 2007).

2.1.2 Modeling Asphalt as a Cubic Material (Yen Model)

There are four peaks in the XRD patterns of asphaltene. The peak γ is thought to be the packing distance of saturated structures which arises from x-ray scattered by aliphatic chains or condensed saturated rings. The graphane peak or peak (002) comes from the diffraction of x-ray by the stacks of aromatic molecules (Siddiqui et al., 2002). The peaks (100) and (110) in the diffraction of x-ray are from the in plane structure of the aromatics (see figure 2.7). They correspond to the first and the second nearest neighbours in the ring compounds.

The broader the peaks in the XRD patterns, the more short range order and less long range order that exists in the structure type. In general, sharp narrow XRD pattern peaks are from highly crystalline samples with a high degree of long range order. In the case of asphaltene, there is a good long range order in some directions
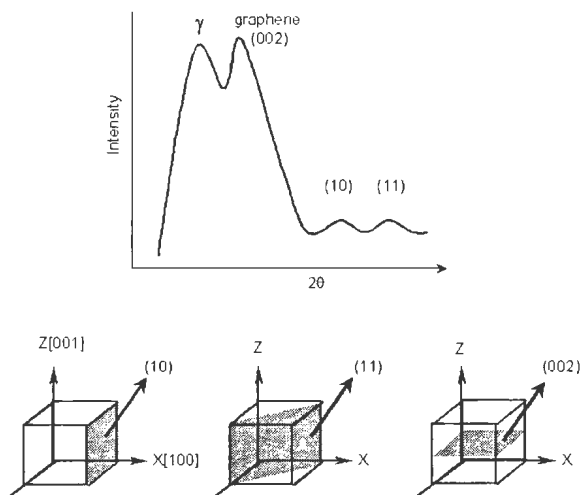
Figure 2.7: The bands (a) and planes (b) of an X-ray diffractogram (Siddiqui et al., 2002).

in the solid crystals, and only short range order in others. This is why there are some sharp peaks and one broad peak in all the diffraction patterns.

2.1.3   The Modified Yen Model (Yen-Mullins Model)

Research on asphaltene structure, molecular weight, and properties, has been revolutionized in recent years. In 2010, Mullins investigated and showed that the uncertainities, particularly the molecular weight of asphaltene, is dramatically improved. Many studies have been conducted utilizing different techniques to uncover or at least to improve the uncertainities of the molecular and colloidal structure of asphaltenes for the past several years. However, it is obvious that, the more one goes deeper in studying asphaltene's structural and chemical properties, the more challenging it becomes, due to asphaltene's complex structure (see figure 2.8).

The modified Yen model, however, gives us a way of designing, handling and analyzing an enormous amount of data. Currently, research on asphaltene is active and reaching

Figure 2.8: The modified Yen Model (Mullins, 2010).

beyond familiar applications to enhance major new objectives in resource utilization (Mullins, 2010). As a result of this achievement, employing the modified Yen model, asphaltene science, can be approached on a first principles basis in part associated with bulk asphaltene properties, thereby simplifying analysis (Mullins, 2010).

Recently, Mullins and co-workers (2012) further investigate and conclude that asphaltene nanoscience model is correlated with the modified Yen model. We do believe that this finding dicloses and solves the existing problem of asphaltene at the nanoscale where most compounds relatively behave consistently, such as the structure, compstion and phase behaviour of asphaltene (see figure 2.9).
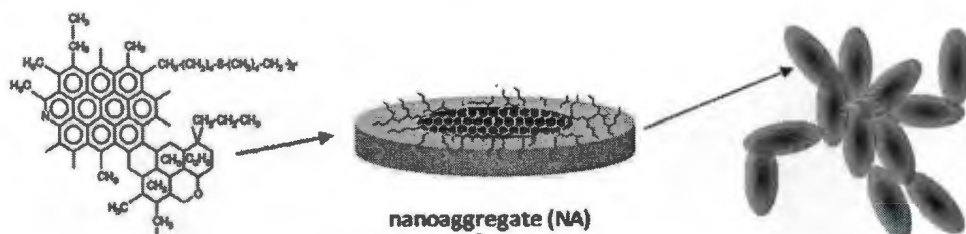
Figure 2.9: An altered figure of asphaltene nanoscience showing consistency of phase behaviour of asphaltene from the modified Yen model.

2.2 Experimental Investigations of Asphalt Binder

Table 2.1 is the summary of what has been done in various studies in the last ten years in expermental investigation of asphaltene in the area of asphaltene science.

Scientific issue	Range of reported values (as of ~1998)	Values (as of 2010)	Width of distribution (as of 2010)
Asphaltene molecular weight	Less than 1,000 Da to 1,000,000,000 Da	750 Da	400–1,000 FWHM
Number of PAHs in an asphaltene molecule	1 to 20	1 dominates	Small mass fraction with 0, 2, 3, etc., ring systems
Number of fused rings per PAH in asphaltene	2 to 20	7	4–10
Number of PAH stacks in asphaltene nanoaggregate	Unknown	1	—
Aggregation number of nanoaggregates	10–100	<10	4–10
Critical nanoaggregate concentration of asphaltenes	50 mg liter^{-1} to 5 g liter^{-1}	100 mg liter^{-1}	50–150 mg liter^{-1}
Concentration of cluster formation	Unknown	~3 g liter^{-1}	2–5 g liter^{-1}
Size of cluster	Unknown	6 nm for small clusters	Probably larger clusters also depending on temperature, concentration
Role of resins in asphaltene nanoaggregate	None to necessary	~15% of crude oil nanoaggregates are resins; resins are not surfactants	Depends on definitions
Relation of nanoaggregate to cluster	Unknown	Clusters consist of nanoaggregates	—
Relation of nanoaggregates in toluene to those in crude oil	Unknown	Very similar in size and composition	—

Table 2.1: Asphaltene Science for the past 10 years, courtesy of (Mullins, 2010).

It has been established that the structural unit of asphaltic substances is an aromatic structure consisting of condensed benzene rings with the inclusion of heterocyclic rings, forming a flat sheet with side substituents, i.e., alkyl chains and naphthene rings, arranged around the edges (Sergienko, 1964). Interaction of the sheets of the individual structural units leads to the formation of particles in which the sheets of condensed aromatic hydrocarbons, being located parallel to each other, form a pile that is surrounded by aliphatic chains and naphthenic rings.

In x-ray structural studies of asphaltene, the presence of particles with an ordered

arrangement of aromatic carbon atoms presence on the diffractograms of asphaltenes as a peak in the region 20°-26° (Cu-Kα-radiation), this peak being observed for graphite which corresponds to the reflection of (002) band from the parallel layers of carbon atoms. However, on this peak there is superimposed a noise scattering from the disoriented carbon atoms, as well as scattering from partially ordered aliphatic i.e. Methane and alicyclic (non-aromatic character) groupings, i.e., γ band. Jen et al. (1961) reported that, in the range of large angle regions, at 20°-43° and 20°-78°, the x-ray diffractograms reveals the peaks of respective reflections (100) and (110) bands from the two dimensional (2D) flat sheets of saturated aromatic hydrocarbons.

2.2.1 Aging of Asphalt Binder

The aging of asphalt is one of the major factors responsible for the deterioration of asphalt pavements in roads and also decreases under heavy traffic conditions. The aging procedure of asphalt binders has been extensively studied by Bell, (1989). The majority of these procedures involve temperatures of 100°C-200°C. The author found out that that correlation of following laboratory procedure relative to field aging was almost made on the basis of a limited number of factors left not considered, such as softening, penetration, etc.

In this research we observe and analyze (using XRD and GFF analysis) the aging effects of asphalt binders caused from improper aggregates (mix) and weather changes in the Canadian petroleum asphalts that have been used to construct all transportation routes. Hesp et al., (2007) found out that x-ray diffraction have shown wax content is a major contributing factor to the reversible aging process (Figures 2.10 and 2.11). Furthermore, they reported, at low temperature condtionaing, small and large clusters of asphaltene sheet size are also reasons for grade loss during condition-

ing at low temperatures.
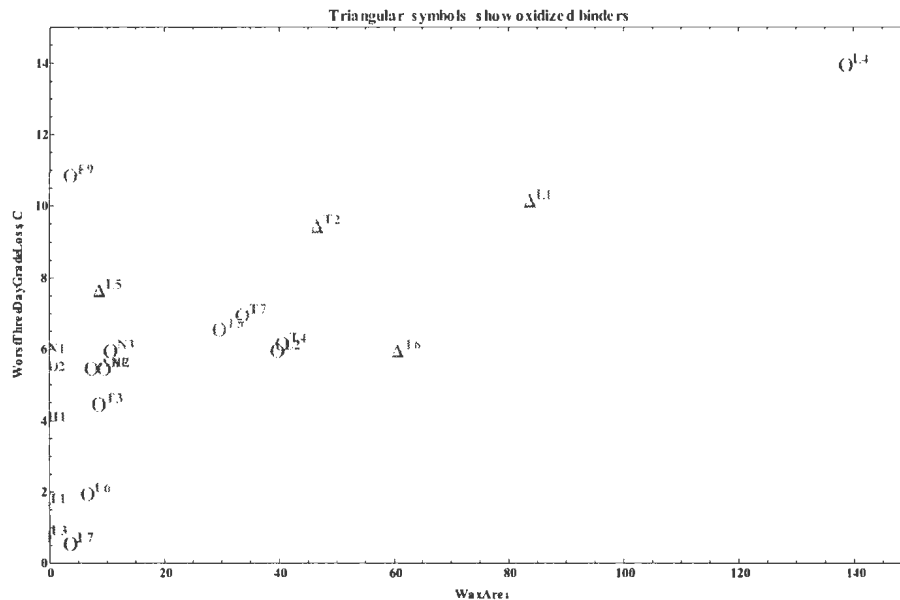
Figure 2.10: Modified wax area in the x-ray diffraction spectrum during Worst three day grade loss (Hesp et al., 2007).

Dow (1903) studied that all bitumens undergo a more or less rapid change with aging where two major causes are responsible:

a) Surface hardening, which is likely due to aging, and possibly due to the evaporation of some light oils. The process starts at the surface and gradually penetrates into the bitumen.

b) Hardening of the entire mass, that occurs due to condensation of molecules. Both these changes take place in all bitumens.

Furthermore, Brown (1958) suggested that when asphalt oxidizes in the pavement, some of the oils and resins surge into the subgrade of the pavement, but the major aging process is that of oxidation. Over the course of aging, the non polar oils remain substantially unchanged, as a result the resins decrease, and the asphaltenes increase
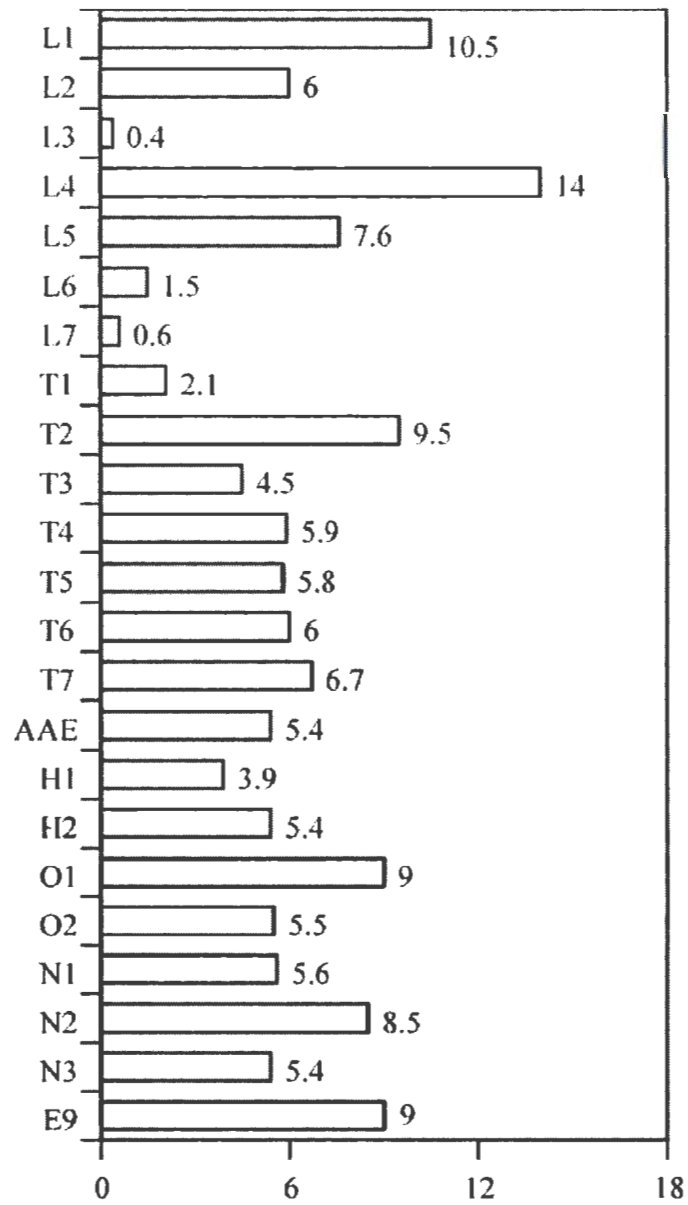
Figure 2.11: Aging of Asphaltene in worst three day grade loss (Hesp et al., 2007).

(Brown, 1958). This shows conversion of the smaller resin molecules to the larger asphaltene molecules.

On the other hand, the long term aging is affected by exposure to high temperature and rainwater also depends on asphalt binder in different geographical locations. Asphalt binders do change their physical and chemical properties due to aging process with respect to time (Philip et al., 1994). Short term aging occurs during the mixing, paving, compacting and long term aging during transportation service, in the case of highways. The rolling thin film oven test (RTFOT) has been accepted as a reliable procedure mostly in evaluating week old aging.

The hardening of petroleum asphalt used in road construction due to slow oxidation is one of the major factors that limit the life of asphalt surfaces and re-surfacings. As this process may take long period of time to become significant and varies depending on the origin of asphalts, and the demography with an accurate means of modeling and ultimately predicting asphalt performance is very important. Road asphalts in cold temperate climates such as Canada, rarely reaches temperatures in excess of 60°C. In the laboratory, modeling of the age hardening process is, however, usually carried out at much higher temperatures in order to obtain data within a practical period.

Correlation between long term aging of asphalt in the field and high temperature laboratory aging have in particular, a tendency toward increased average molecular weights and changes in fractional composition (Yapp et al. 1991), namely a trend to increased levels of the more polar fractions. Petersen and his collaborators (1981) have studied in detail the formation of oxygen containing functional groups during oxidation of 15 part per million (ppm) films at 130°C. This and other work related to asphalt composition and durability has been reviewed by Petersen (1984). Results for laboratory-aged (24 h, 130°C, 15 ppm films) and the same field aged asphalt extracted

from eleven to thirteen year old asphaltic concrete cores were compared (Petersen, 1984). Agreement was generally improved significantly given the likely variation in air void content of the mixes and the importance of this factor in asphaltic concrete oxidation rates (Petersen, 1989). However, (Petersen, 1989) the significance of 130°C asphalt aging is questioned on the basis of differences in the availability of reactive species compared to standard temperatures. In the field slow reversible molecular structuring may act to sterically hinder possible reaction sites.

As asphalt source and the tendency for steric hardening is related, comparison of oxidation rates at high temperatures may lead to errors and wrong conclusions. This would have the effect of reducing the rate of reaction in the field compared to that at high temperatures beyond that expected from the simplest Arrhenius temperature dependence equation:

$$K = A \exp[-E_a/RT] \tag{2.9}$$

Where,

A is constant

R universal gas constant

T asolute themperature in Kelvins

E_a actvation energy

Furthermore, asphalt aging is having a tendency to go delicate and stiff due to exposure to heat, oxygen, and UV light during storage, mixing, transport and laying down, as well as in service life. These aging processes lead to decrease of asphalt properties as mensioned in introduction section such as high temperature rutting and low temperature cracking, and shorten the lifetime of pavement. The photochemi-

cal transformation of asphalts must be considered in the study of the performance of asphalt pavement, especially in geographical regions where high solar radiation intensity occurs, for example Africa.

Many methods have been applied since, to investigate the process of asphalts aging and where the majority of the study applied standard rolling thin film oven (RTFO) test to simulate the short term aging of bitumen. The aging asphalt is simulated using two of the major mathematical functions (Pseudo-Voigt and Pearson VII). Using real aging asphalts from the specimen. Periodically, the XRD profiles were calculated and the results analyzed. The XRD showed be possible differentiate asphalts of different standards classifications through peak centroid and others parameters.

One of the important factors determining the lifetime of constructions in which asphalt has been used is the influence exerted on the asphalt by the weather. The entire complex of changes in the properties of asphalt by atmospheric influences, to the detrament of the construction concerned, is called aging. The aging phenomena of asphalt is extensively studied by Yu et al., (2009).

Frequently, correlations between aging phenomena and properties of the asphalt are sought by purely empirical methods. Many methods described aim at obtaining direct information by short time tests on asphalt behavior after long exposure. According to the literature, the action of oxygen is one of the principal factors responsible for the occurrence of the aging process. When asphalt is exposed to atmospheric oxygen, the chemical nature of which depends to a very large extent upon the temperature will experience change.

Shenoy, (2002) showed that at temperatures above 100°C., dehydrogenation takes place, as is evident from the water produced and also carbon dioxide formed. At lower temperatures such as, 25°C or 50°C, the oxygen involved in the oxidation is quantitatively bound in the bitumen and no water or carbon dioxide is formed. The

rate of the oxidation may be followed by means of oxygen absorption measurements. The overall rate of oxygen absorption was found to be not only determined by the chemical nature of the asphalt, but also by the physical transport of the oxygen from the surrounding atmosphere to the interior of the material. Therefore, it is also a physical problem, one of diffusion in particular.

Asphalt binders age mainly due to two main mechanisms:

(a) volatilization of light oils present in the asphalt.

(b) oxidation by reacting with the oxygen in the environment.

The blending and agitation in the hot mixing facility and during placement ages the binder by both mechanisms because of the high temperature and air flow involved in the process. In this work, the rolling thin film oven (RTFO) procedure is used to simulate this form of aging. After the asphalt pavement is constructed, aging continues, but the oxidation mechanism dominates because of the relatively moderate temperatures of the environment Lee, (2009).

2.2.2   Modeling Asphaltene

The modeling of asphalt concrete is an active area of research to make an efficient performance of pavements. Continuing developments and improvements on uncertainities in computational power and test techniques allow asphalt materials and pavement expertise to implement more realistic, powerful models to predict the performance of asphalt materials, pavements, and microstructure (see figure 2.12).

The detection of bubble points and asphaltene aggregation onset pressures by near infrared spectroscopy (NIR) for both a live crude oil and model systems has been demonstrated by Narve et al., (2002). The aggregation onset pressure is seen as a baseline elevation of the NIR spectra due to light scattering.
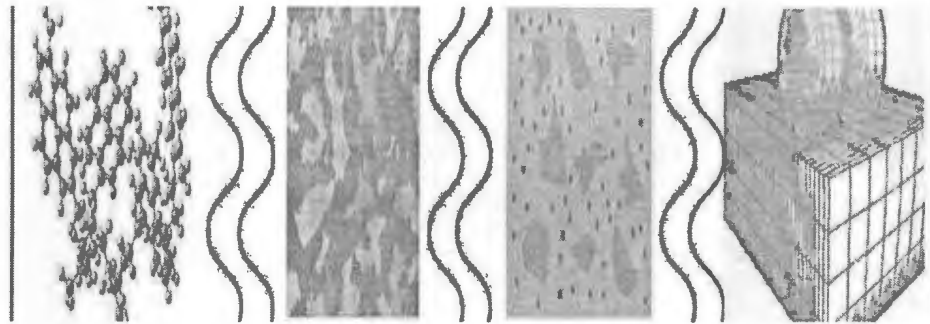
Figure 2.12: Asphalt Binder Microstructure (Pauli, 2010).

The asphaltene aggregation from a live crude oil has been shown to be more or less completely reversible, although 72 h of equilibration was needed to completely redissolve the asphaltene aggregates. The results obtained by Narve et al. (2002) showed that the non precipitate of asphaltene aggregates formed by pressure depletion of model asphaltene systems was only partially reversible. Obtaining a good model of asphaltene at the microscopic level has enormous impact on the macroscopic model of concrete pavement. Asphalt concrete pavement, is a complex system that includes many layers of different materials, various combinations of irregular traffic loading, and varying environmental conditions. Therefore, a realistic prediction of the long usability of asphalt pavements is one of the most challenging tasks for pavement engineers Kim (2008). The performance of asphalt concrete pavements is closely related to the performance of asphalt concrete. It is performance models of asphalt concrete that provide the links among various processes involved in asphalt mixture design, pavement design, construction, and rehabilitation.

Some of the factors that affect the deformation behavior and performance of asphalt concrete are aging, moisture, temperature and model of loading. Kim (2008) described that many asphaltene models have been developed to capture the effects of

these factors on asphalt concrete performance. Most of these models, developed before the Strategic Highway Research Program (SHRP), are empirical in nature. The importance of mechanistic models for material specifications, mixture design, and pavement design and developed a range of research products based on the principles of mechanics. The evolution from using empirical to mechanics during the SHRP made a significant impact on the role of models in asphalt pavement engineering Kim (2008).

2.2.3 Precipitation of Asphaltene

Hussam et al., (2004) investigated that asphaltene precipitation rate dependence on asphaltene content of the oil decrease as the heteroatoms content of both the crude oil and asphaltenes increased. However, asphaltene precipitation increase as the aromatic carbon fraction and the degree of branching of the asphaltene molecules increase. On the other hand, asphaltene precipitation rate dependence on the amount of n-heptane (i.e. light paraffin hydrocarbon) added decrease as the paraffin fraction of the asphaltenes increase, but increase as the propensity of the asphaltene molecules for aggregation increase Hussam et al. (2004).

Groenzin and Mullins, (1999) reported that asphaltene molecular weights are known to be, 800 g/mol. Asphaltene science performed at different length scales (such as nano scales) into a standard picture requires establishing structural relationships is the major part of Petroleomics (Mullins et al., 2007). Compositional variations of the fluid containing asphaltenes directly affect their aggregation state. In addition, asphaltene molecules tend to associate into small nanoaggregates that are changed into larger clusters and eventually precipitate. Mullins, (2010) found out clear description of the connection between molecular architecture and aggregation

of asphaltene. Furthermore, the role of resins specially on asphaltenes' stability has long been controversial, however, a more unified view is emerging (Goual et al., 2011). This is based upon the author's (Goual et al., 2011) experience in asphaltene research over the past decade. It focuses on asphaltene separation, characterization, structure and role of resins.

Nikhil and co-workedrs, (2001) reported asphaltenes of different characteristics are found to precipitate at different pressures. Decreasing the pressure forms small amount of flocs and , initially formed flocs are remain unchanged. This characteristic shows that asphaltenes are stable and should be resin deficient. Latter flocs are likely to have more resin and be tackier thereby having an adverse effect on crude oil production. Furthermore, these authors revealed that field asphaltene precipitation is shown to be largely reversible with pressure over a certain time (minutes). It is worse to recognize that asphaltenes extracted by pressure reduction on live crude oil are quite different to those prepared by solvent precipitation from dead oils. However, most authors use the same terminology, called asphaltene in both cases.

Asphaltene precipitation in crude oils can occur not only by adding solvents such as heptane but also occurs at elevated temperatures. Therefore, self-precipitation of asphaltene in crude oils with different compositions occurs at different temperatures, Bayat et al. (2008). This phenomenon is only dependent on the composition compatibility of the oil, and it does not depend on the asphaltene content. Because of the composition compatibility, heavy crude oils with high asphaltene content may be more stable than light ones with low asphaltene content.

Tharanivasan et al., (2009) found out a method to use what they called (regular solution approach) to model asphaltene the onset and amount of asphaltene precipitation from their prepared specimen diluted with n-heptane. These author's showed that the composition of the samples could be determined using a mass average of

the crude oil of saturates, aromatics, resins and asphaltenes (SARA) analysis. The average aggregation number of the asphaltenes was a molar average of the crude oil asphaltene aggregation numbers. Finally, the molar mass distribution of the asphaltenes in the prepared specimen was determined by adding the mole weighted distributions from crude oil and obtained a result indicating the asphaltenes from different crude oils did not interact with each other for short time scale. To generalize the method developed, the results require to be tested over longer time scales, the data support models that assume no such interaction.

However, the model successfully predicted the amount of heptane required to precipitate asphaltenes in a range of blends and also predict when blends are less stable than the constituent crude oils. But, the model was less successful at very high asphaltene dilutions, for example, when toluene had been added to the crude oils prior to heptane addition. At these level of dilutions, asphaltenes tend to dissociate, and the assumption that the average asphaltene aggregation number is constant doesn't work, Tharanivasan et al., (2009).

A good background of understanding under what conditions the asphaltenes precipitate and to what extent precipitated asphaltenes can be redissolved is very important. Although there is considerable data available in the literature on asphaltene precipitation, Peramanu et al., (2001) studies mostly focus on the measurement of the ratio of solvent to bitumen at which asphaltenes begin to precipitate. There is limited data available on the effect of the reversal of solvent concentration or temperature on asphaltene precipitation. And yet, data on reversibility of asphaltene precipitation is essential for bitumen or heavy oil processes that involve solvent addition and recovery. Furthermore, these data help in investigating the validity of asphaltene precipitation models based on solution thermodynamics Peramanu et al., (2001). For instance, the theory of thermodynamics predict that asphaltene precipitation is fully reversible

while the colloidal theory predicts irreversible precipitation.

2.2.4 SAXS and SANS

Herzog et al. (1988) performed small-angle x-ray scattering (SAXS) experiments using a synchrotron x-ray source for some asphaltene dispersions in organic solvents as well as natural solvents (maltenes). They interpreted asphaltene species as thin, large and porous particles with varying radius and a lateral extension possibly greater than 80nm.

This interpretation has been supported by several other experimental observations including those by Xu et al. (1995), who used SAXS to demonstrate the existence of particles with sizes ranging from 3 to 15nm in crude oils diluted in aromatic solvents. Small angle neutron scattering (SANS), used by Ravey et al. (1988), revealed particle sizes in this same size range. Also they concluded that the physical dimensions and shape of the asphaltene aggregates was a function of solvent and temperature of investigation. XRD was used by Siddiqui et al., (2002) to investigate the structure characterization and the aging pattern of asphalt binders. Asphaltene has high resistance to cracking. As a result it is difficult to biodegradable, due to presence of heavy metal components. On the other hand, the presence of high percentage of asphaltene has an advantage in obtaining quality pavements in hot and cold locations.

2.2.5 Asphalt Pavement failures

There are four major factors of physical deterioration of asphalt pavement.

a) Rutting (permanent deformation)as mentioned earlier caused by progressive movement of materials under repeated application of loads at high temperature.

b) Fatigue cracking caused by application of loading which exceeds the structural

design criteria.

c) Low temperature thermal cracking caused by the development of thermal stress that exceeds the fracture strength at low temperatures.

d) Moisture damage (stripping) of asphalt pavements caused by the lack of an adhesive bond between the asphalt and aggregate due to the presence of moisture. Stripping is one of the factors that contribute for rutting and fatigue cracking and can lead to disintegration of the pavement.

Asphalt concrete failures caused by low temperature cracking is a big challenges for proper pavement performance and service life (see Figure 2.13).

Early maintenance or replacement of the damaged road is the occasional task by the construction expertise and engineers. The implication on the economic aspect of this maintenance is enormous amount of money for the taxpayers also putting more time waiting for road construction season after season. Therefore, it is crucial to study and understand the critical cracking temperature, for instance in cold region, of the asphalt cement and concrete in order to prevent failures.

On the other hand, laboratory tests that evaluate rutting use the maximum pavement design temperature, whereas tests that evaluate fatigue potential use the intermediate pavement design temperature. However, thermal cracking tests use the minimum pavement design temperature plus 10°C. The minimum pavement design temperature is increased by 10°C to reduce the testing time. These results are corrected to the minimum temperature using the time-temperature shift factor (McGennis, 1994).

At present, rutting is a major kind of damage of asphalt pavement at home and abroad, especially the question of initial rutting of the asphalt pavement. Rutting brings tremendous economic loss to country roads and highways disadvantage to society that needs close attention. At present, The effective measures to improve high
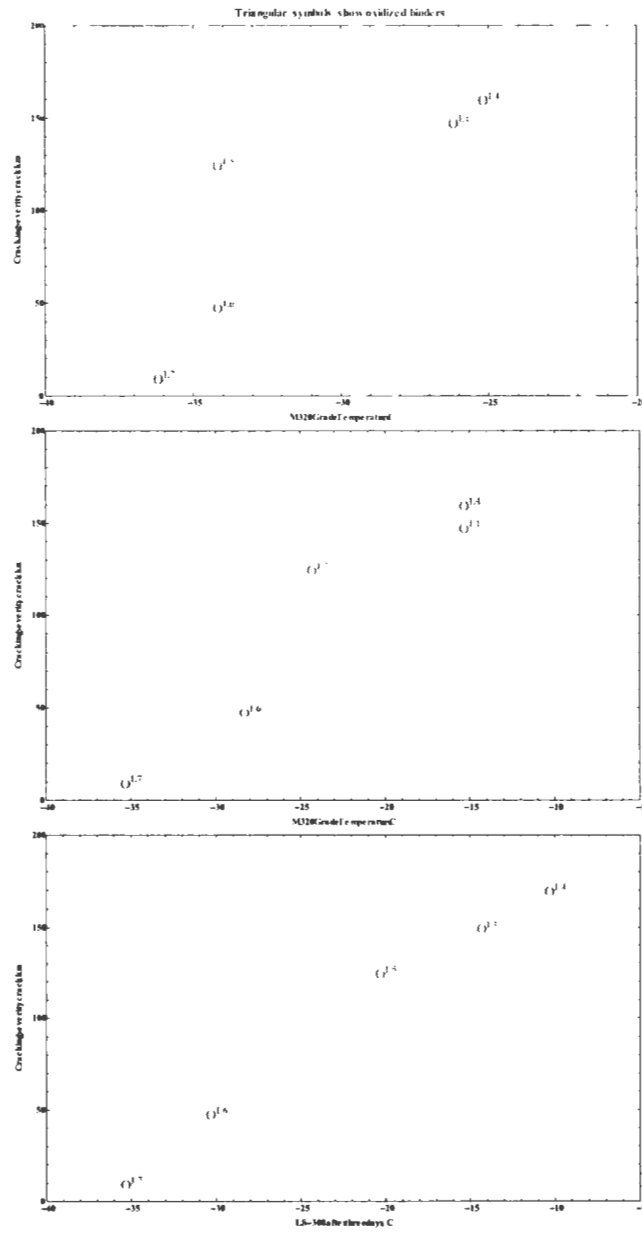
Figure 2.13: Cracking severity versus (a) AASHTO M320 and (b and c) LS-308 grading temperatures for Lamont, Alberta, C-SHRP pavement trial binders (Zhao et al., 2006).

temperature stability performance of asphalt mixtures, the main methods: adjust the aggregate grading of asphalt mixtures, adopt modified asphalt or compound modification asphalt (specially modified asphalt, SMA), strengthening constructional management and quality control of asphalt pavement. Although all of the approaches have furthered development in high temperature stability performance of asphalt mixtures to some extent, do not solve the existing problems. Methods that seek an economical and effective reinforcement method for solving asphalt pavement rutting in subtropical region during the summer is important.

Through these experimental studies, it appears that high viscosity asphalt has the character of high viscosity, low penetration, high softening point and little ductility. The mixture has properties of high intensity, high modulus, perfect high temperature performance, water stability, anti-fatigue property and mechanical property. It is more suited to asphalt middle layer and subsurface at high summer temperature and heavy axial load, which can largely evaluate the high temperature performance, water stability and fatigue life of asphalt pavement. Since they bring greater social and economic benefit, the application prospect of high viscosity asphalt is good.

2.3 Performance Grade and Asphalt Binders testing Methods

One of the objectives of the Strategic Highway Research Program was to develop performance based testing of asphalt binder materials. This research lead to Performance Grade (PG) binder specifications. Traditional methods for evaluating asphalt were largely empirical and the asphalt was only evaluated at two temperatures, the mixing temperature and the maximum service temperature.

Penetration Grades	80-100		120-150		150-200	
Requirements	Min.	Max.	Min.	Max.	Min.	Max.
Penetration at 25°C, 100g, 5s, 0.1 mm	80	100	120	150	150	200
Viscosity @60°C, Pa.s or Viscosity @135°C, mm²/s Group A Group B Group C	User must specify either Absolute or Kinematic Viscosity for all Asphalt Grades (Such as Figure 1) (Both Viscosity requirements shall not be used simultaneously)					
Flash Point (Cleveland Open Cup), °C	230	---	220	---	220	---
Thin Film Oven Test, % loss in mass	---	0.85	---	1.3	---	1.3
Penetration of Residue at 25°C,100g, 5s, 0.1mm, % of original penetration after Thin Film Oven Test	47	----	42	---	40	---
Solubility in trichloroethylene, % by mass	99.0	----	99.0	----	99.0	---

Table 2.2: Canadian General Standards Board (CGSB) Specifications for Asphalt Grades used on Canadian Airports (Chuck, 1999).

Since the properties of asphalt are highly temperature dependent, it was important to cover the entire range of temperatures the asphalt is exposed to over its service life. Table 2.2 shows three asphalt grades (PG) currently recommended for airport pavement construction in Canada. These grades (PG) are identified by their depth of penetration which describes typical characteristics of fatigue cracking and rutting that predict performance characteristics, such as at low and high temperature exposure respectively (section 1.1.3).

Figure 2.14 shows penetration vs viscosity combination of penetration grades. The specification includes requirements for the flash point, penetration of residue as a percentage of the original penetration after the thin film oven test (TFOT), solubility in trichloroethylene, and mass loss by the thin film oven test.

2.3.1 Rolling Thin-Film Oven

The rolling thin film oven is used to simulate hardening (durability) characteristics of asphalt binders (see figure 2.15). The RTFO simulates the thin films of binder as
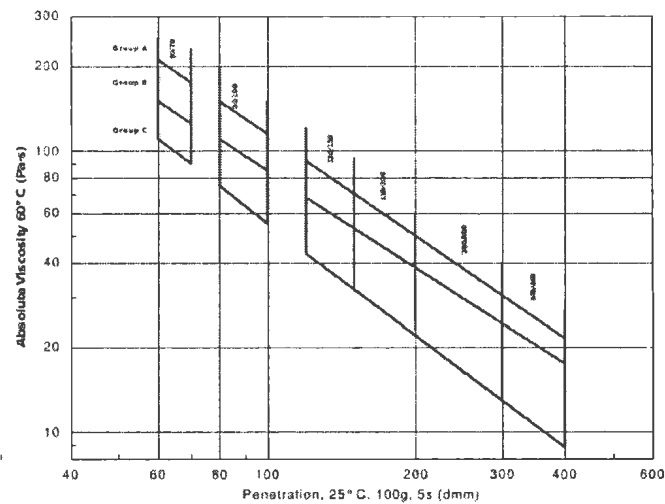
Figure 2.14: CGSB Specification for Absolute Viscosity vs Penetration (Chuck, 1999).

they are exposed to heat and forced air during the mixing process and placement. A sample is poured into a cylindrical bottle and rotated horizontally at approximate mixing temperatures. As the bottle rotates and air is blown over the sample, new thin films are exposed simulating the binder coating on the aggregate during mixing.

Lighter oils are driven off and some oxidation occurs. A mass change determination is made and because RTFO aged asphalt binder is approximately 2-3 times the viscosity of the unaged asphalt binder, it is tested to determine whether the desirable viscoelastic properties have been maintained.

Asphalt binder is rapidly aged during the construction process. Heating the asphalt to mixing temperature and blending it with the aggregates causes rapid oxidation and volatilization. The rolling thin film oven is used to condition asphalt binder samples to simulate the change in binder characteristics during the construction process. After the asphalt is placed, the aging process continues for an extended period of time. The pressure aging vessel (PAV) is used to simulate the hardening that asphalt binder would experience during seven to ten years of service.
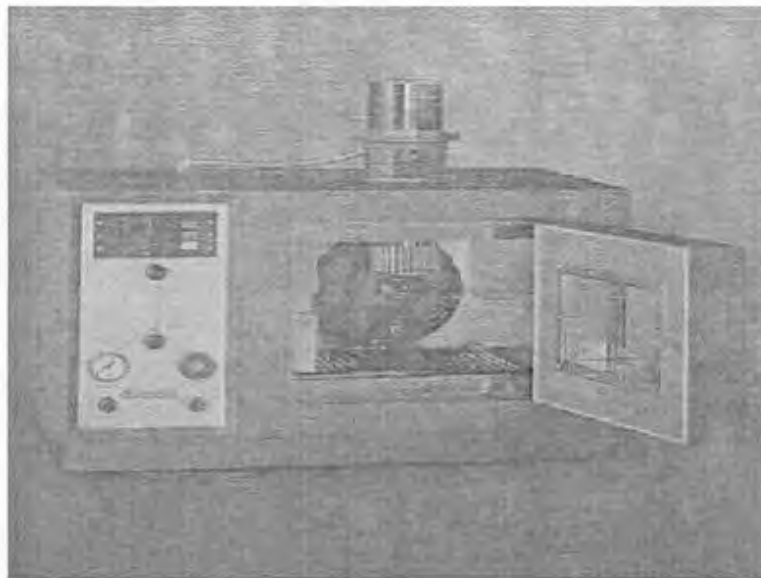
Figure 2.15: Rolling Thin Film Oven for short term aging (McGennis, 1994).

2.3.2   Pressure-Aging Vessel

Simulate hardening (durability) characteristic. Pressure-Aging method (see figure 2.16) is used for testing asphalt binders already aged using the rolling thin film oven (RTFM). the pressure aging vessel consists of controlling devices for: temperature, pressure and measuring devices. Pressure Aging Vessel (PA) engages oxygen before the testing process, hence using a vacuum oven is crucial to avoid any unwanted air bubbles from the specimen.

The device uses pressure and temperature to compress time so that very long term aging can be simulated in only 20 hours. Asphalt binders, after aging in the RTFO, are placed in the PAV and aged for 20 hours. The physical properties are measured to determine if the asphalt will be suitable after several years of service. The test is conducted at different temperatures depending on the climate in which the pavement
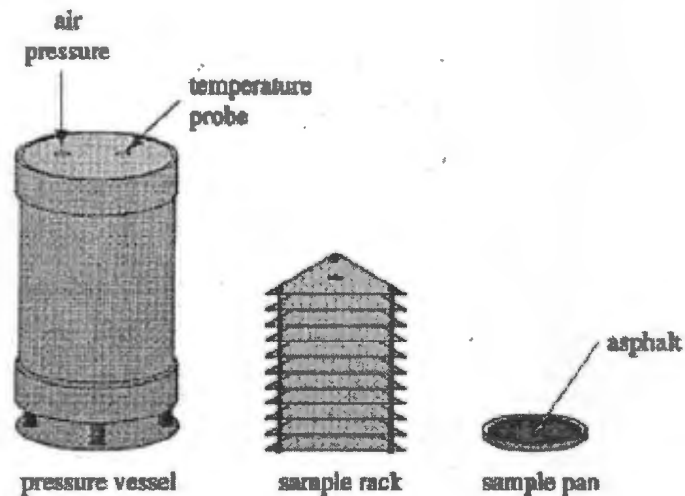
serves.

Figure 2.16: Pressure aging components used for long term aging (McGennis, 1994).

Since the PAV is only an aging instrument, preparation and final result typically contains: Sample identification, aging test temperature to the nearest 0.1°C. Aging temperature and pressure usually recorded at 1 minute intervals from the time pressure reaches 2.00MPa until the 20 hour aging run ends, and 16 minutes to record the depressurization period. Such as, total time during aging that temperature was outside the specified range, total time during aging that pressure was not at 2.10MPa and total aging time.

One of the limitations of some of the older grading systems is the inability to simulate actual aging conditions of asphalt binder as it goes through production, mixing placement and, particularly, long term aging. After mixing and placement, further oxidation will occur over the service life of the pavement. The PAV was refined during the Strategic Highway Research Program (SHRP) to subject asphalt binders

to the long-term aging expected after 5-15 years of service in an asphalt pavement. Asphalt Binders are exposed to high temperature (100°C) and air pressure (2.07 MPa) for 20 hours to simulate long-term aging. Resulting viscosity of the PAV-aged asphalt binder is approximately eight times the viscosity of the unaged asphalt binder.

2.3.3   Bending Beam Rheometer Test

In general, BBR measures properties at low temperatures (see figure 2.17). When the pavement temperature drops, two simultaneous events occur that are detrimental to pavement performance. The reduction in temperature causes a volume reduction which due to the constraining effect of the pavement slab, generates stresses in the pavement. Concurrently, the drop in temperature causes the asphalt stiffness to increase making the binder more susceptible to cracking due to the thermal stresses. The bending beam rheometer (BBR) evaluates the binder's ability to resist thermal cracking. Since the potential for thermal cracking increases when the asphalt stiffness increases due to age hardening, the BBR test is performed on samples that have been conditioned in both the rolling thin film oven and the pressure aging vessel.
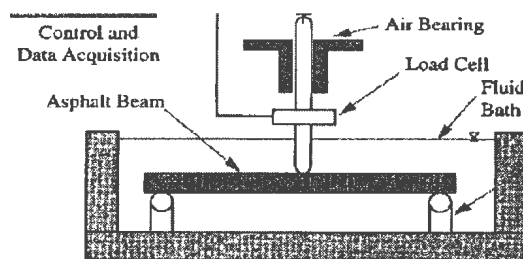

Figure 2.17: An Altered Figure of a Bending Beam Rheometer (LS-298, 2005).

BBR is used to measure the flow properties of liquid asphalt binders at low (i.e. -12° C) temperatures. It is analogous to the DSR which is not used at low temperatures because of the torque capability of the equipment. The BBR operates on engineering

beam principles, such that a fixed static load is applied to an asphalt binder beam of known dimensions. The resulting deflection is measured and the flexural stiffness reported as a function of time. Provides an indication of the low temperature stiffness and cracking potential of an asphalt binder.

2.3.4   Direct Tension Test

Roberts and his colleagues (1996), measure failure properties of an asphalt binder at low temperatures, especially from 0°C to -46°C range. It provides an indication of the failure stress and strain of an asphalt binder. The Direct Tension Test was originally used as a referee test when the m-value from BBR results passed but the estimated stiffness failed and was between 300 and 600 MPa. If the average strain value from the DTT was one percent or more, it could be assumed the binder was sufficiently elastic at the tested low temperature range.
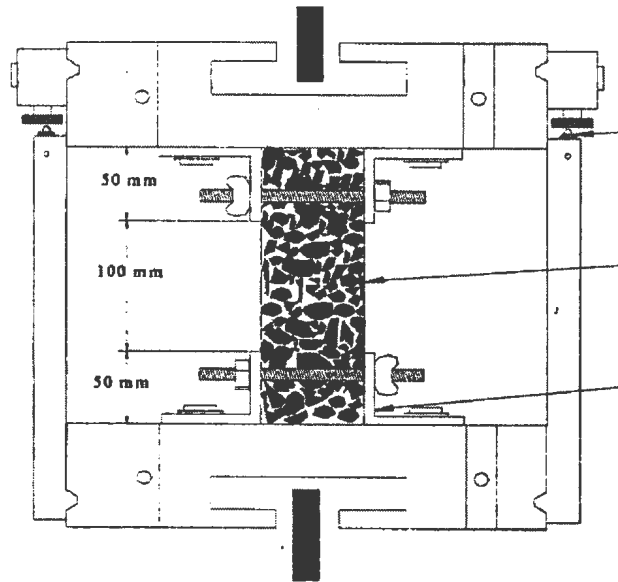

Figure 2.18: An Altered Figure of Direct Tension Test.

More recently, the Direct Tension is being implemented as one test in the determination of low temperature critical cracking (see figure 2.18). Used in conjunction with the Bending Beam Rheometer and software that incorporates the data from both tests we are able to better characterize low temperature binder properties. The critical cracking temperature is considered to be the point at which the maximum stress at a given temperature exceeds the strength of the material.

2.3.5   Rotational Viscometer Test

The Rotational Viscometer measures asphalt viscosity at the mixing temperature (see figure 2.19). This device measures the force required to rotate a spindle at a constant speed while the asphalt binder is kept at the required test temperature. This device replaces the kinematic viscosity test. The Rotational Viscometer and the kinematic viscosity tests measure the same property and are interchangeable. The Rotational Viscometer is preferred for ease of operation.

Figure 2.19: The Rotational Viscometer measures asphalt viscosity at the mixing temperature (www2.cemr.wvu.edu, 2000).

It measures viscosity (kinematic) at high temperatures as high as 135°C. It is used in mix designs to provide representative temperatures for mixing and compaction of asphalt mixtures. It operates as a rotating cylinder within a fixed sample cylinder (within a thermal-controlled chamber). Resistance to flow is measured as the torque applied to a spring and converted to viscosity.

2.3.6 Dynamic Shear Rheometer Test

The dynamic shear rheometer (DSR) measures the viscoelastic properties of the asphalt cement at the highest pavement temperature and at an intermediate temperature (approximately the average of the high and low temperatures; see figure 2.20). The DSR applies a sinusoidal load to a plate shaped sample. The deformation response of the sample is measured and the shear stresses and shear strains are determined. These are used to compute the complex modulus and the phase angle of the asphalt binder. The test at the higher temperature evaluates the ability of the asphalt binder to resist permanent deformation (rutting) of the pavement. The developers of
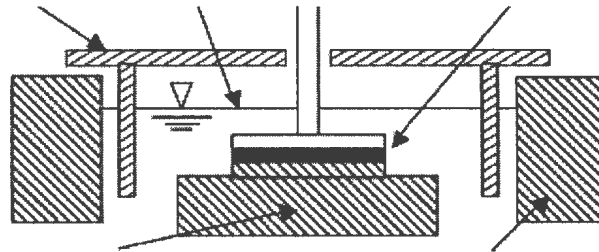

Figure 2.20: An altered schematic diagram of Dynamic Shear Rheometer (Gordon, 2002).

the PG specification hypothesized that rutting potential is critical at high temperature and during the initial pavement performance period, before the binder stiffness increases through age hardening. Thus, the high temperature tests are performed on

samples which have been conditioned with the rolling thin film oven.

The SHRP researchers hypothesized that the critical time for fatigue is after the asphalt has age hardened and when the temperature is in the intermediate range. Thus, the tests at the intermediate temperature are performed after the samples have been conditioned with both the rolling thin film oven and the pressure aging vessel Also known as an oscillatory shear rheometer, it is used to measure the flow properties of liquid asphalt binders at intermediate (i.e. 20°C) to high (i.e. 64°C) temperatures. It works by applying a sinusoidal shear stress to produce a resulting shear strain. The complex shear modulus (G^*) is a ratio of the applied shear stress (t) to the resulting shear strain (g). The phase angle, d, (related to the time lag between input and output signals) provides a relative indication of the viscous and elastic behavior of the asphalt binder. Materials with a phase angle of 90 degrees are completely viscous; while materials with a phase angle of 0°C are completely elastic. At intermediate temperatures, such as 20°C, asphalt binders are said to be viscoelastic (phase angle near 45°C).

2.3.7 Microscopy

Fluorescence and phase contrast images have been obtained on asphalt binder samples using the latest techniques in optical microscopy to identify variations in chemical phases in asphalt binders (see figures 2.21 to 2.23; Hesp et al., 2007).

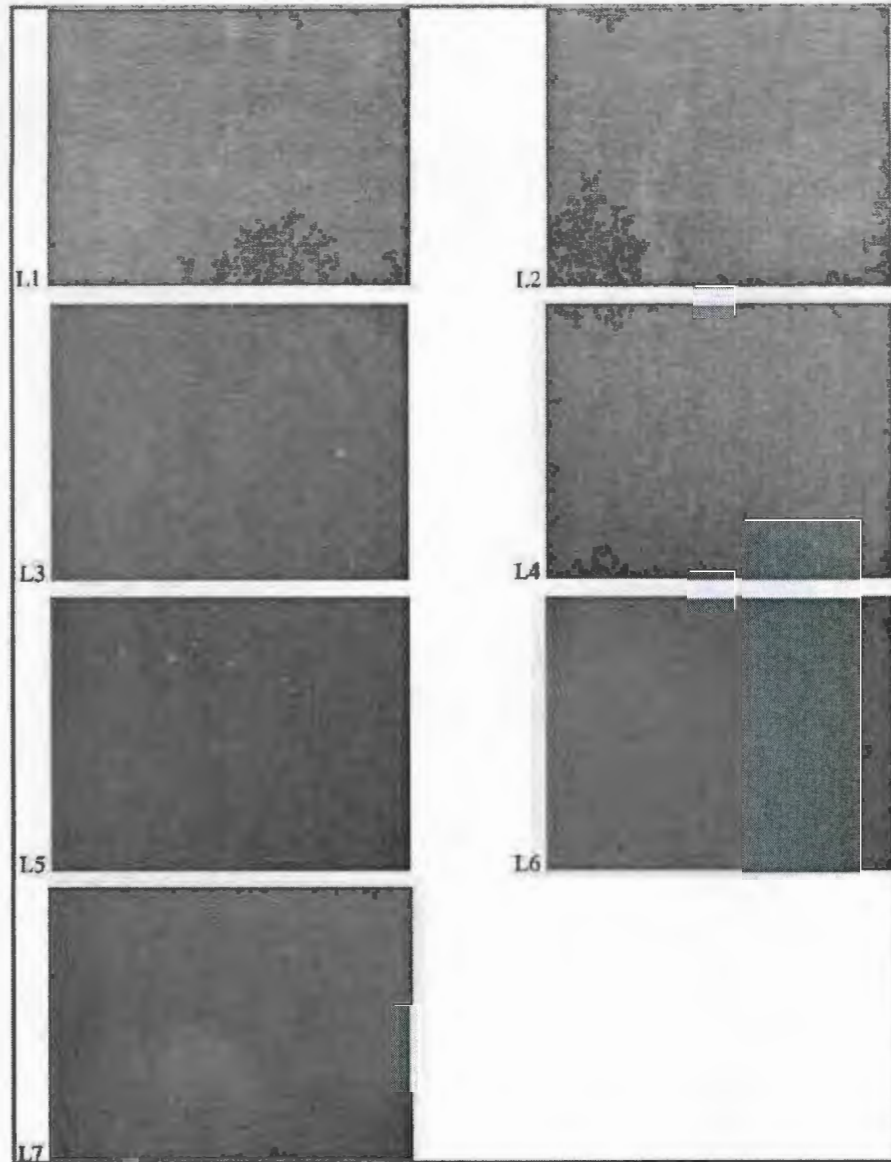Figure 2.21: Fluorescence (dark grey) and phase contrast (light grey) images of Lamont, Alberta, C-SHRP binders (Hesp et al., 2007).
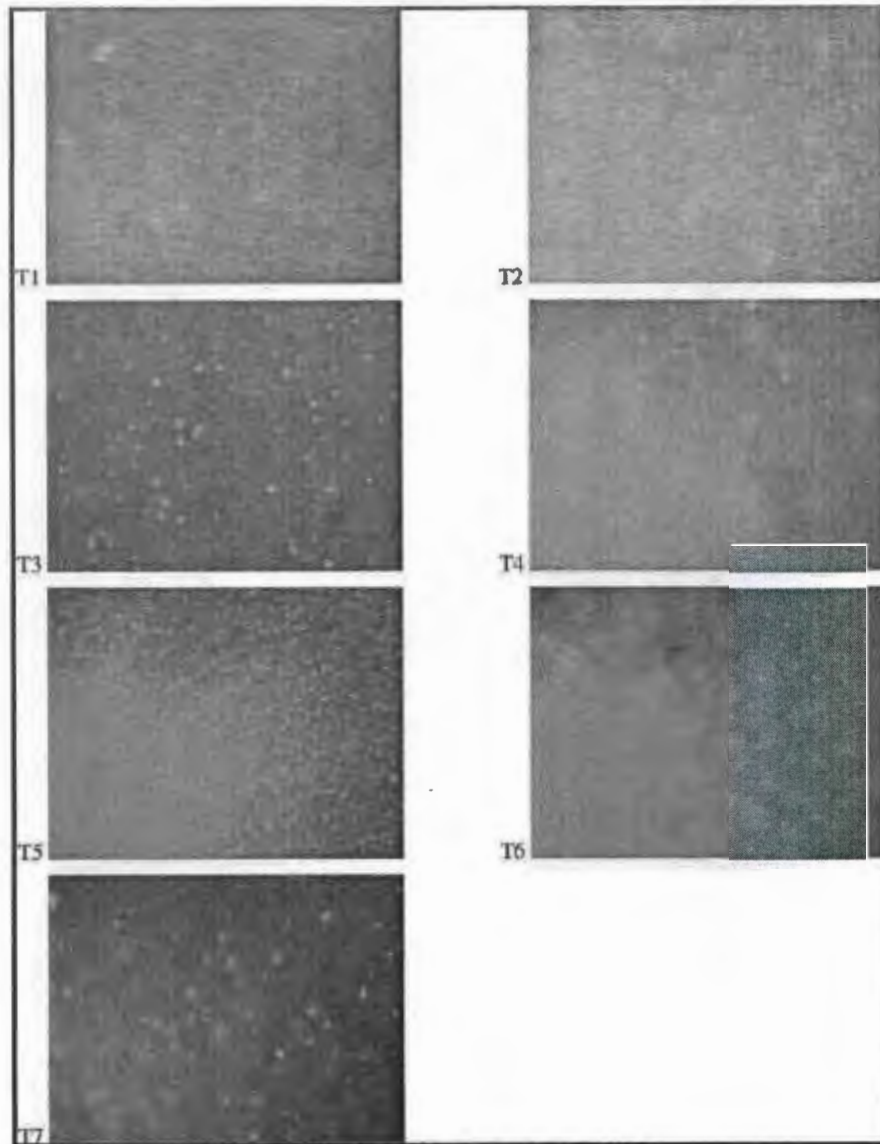
Figure 2.22: Fluorescence (dark grey) and phase contrast (light grey) images of the Timmins, Ontario, trial binders (Hesp et al., 2007).
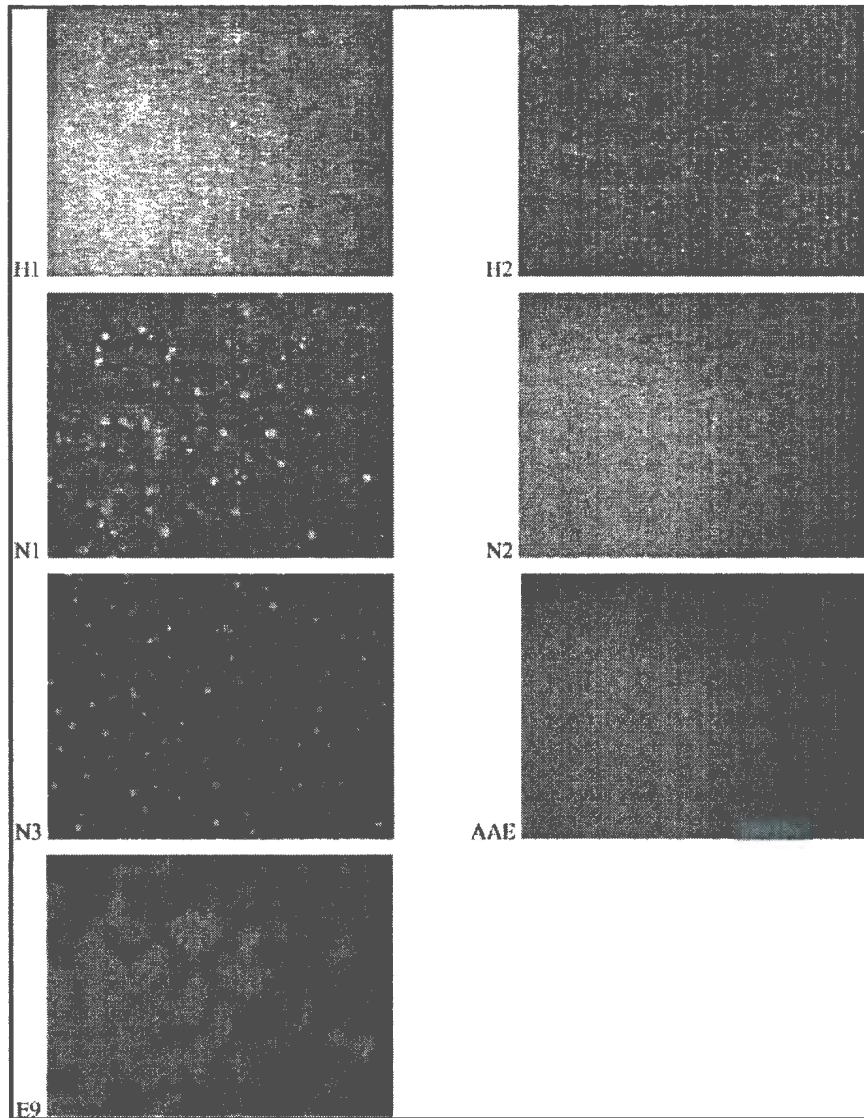
Figure 2.23: Fluorescence (dark grey) and phase contrast (light) images of miscellaneous asphalt binders (Hesp et al., 2007).

Chapter 3

Experimental

3.1 Set-up Components

Most of our knowledge of the internal structure of amorphous and crystalline solids is derived from x-ray diffraction studies. The crystallite structure of asphaltenes can be determined by using XRD. For diffraction to occur in a crystal in which atoms are arrayed in planes, the wavelength of the incident radiation must be of the same order as the atomic space distances between crystallographic planes. Figure 2.3 showed in cross section two x-rays of wavelength impinging at an angle θ on the surface of an asphaltene cluster in which aromatic sheets are arrayed in planes separated by an interplanar distance d_M. The planes with a relatively large number of atoms on them usually give rise to strong reaction of the incident x-rays.

XRD provides macrostructural information and the crystallite parameters of the molecules associated in the asphaltene aggregates. XRD gives quantitative intensity curves, and structural parameters can be obtained from the shape and the position of the peaks (Trejo et al., 2007). The more amorphous the material under investigation, the more peak broadening is observed in the diffraction patterns. Various parafins,

naphthenes and aromatics of XRD patterns indicated that the gamma band (γ) is thought to arise primarily from aliphatic side chains or aliphatic ring ordering; the graphene (002) band, which comes from stacks of aromatic molecules, and the (100) band corresponds to the nearest and second-nearest neighbors in ringed compounds (Sadeghi et al., 1986). The significance of the gamma (γ) band is that it represents the packing distance of aliphatic chains or the layer of condensed saturated rings (Siddiqui et al., 2002). The x-ray techniques used in this work are those of Yen et al. (1961) and Sadeghi et al. (1986), used previously in studies of asphaltenes. The crystallite parameters such as the interlayer distance d_M, the interchain distance, d, the diameter of the aromatic clusters L_c and the diameter of the aromatic sheets L_a were obtained from the x-ray diffraction patterns of the Canadian asphaltenes.

The x-ray intensities measured over the range $2\theta = 3°$ to $90°$. The curves exhibit qualitatively similar peaks. The studies in the literature (Sadeghi et al., 1986; Siddiqui et al., 2002; Yen et al., 1961) showed that the asphaltene XRD pattern has 4 main characteristic bands, the gamma band (γ), the (002) band, the (100) band and (110) band.

The XRD patterns of the Canadian asphaltenes examined in the present work has the same features as those reported in the literature (Sadeghi et al., 1986; Siddiqui et al., 2002; Yen et al., 1961). As shown in chapter 4, the XRD patterns of Canadian asphaltenes are very similar and have three characteristic peaks which give three maxima approximately at $20°$ gamma (γ), $25°$ graphene (002), and $44°$ (100). Also, a weak indication of a broad peak (110) centered at approximately $2\theta = 80°$ is observed. These broad features indicate that the ordering is very dispersed in the asphaltenes (Andersen et al., 2005). The average distance, indicated by the maximum of the graphene band (002), which is located around $25°$ in the 2θ axis, between the aromatic sheets, d_M of asphaltenes was calculated by the Bragg equation, $d_M = \lambda/2\sin\theta$, where

λ is the wavelength of Cu-K-α radiation, and θ is the Bragg angle. The (002) peak is positioned around $2\theta = 25°$, indicating an interlayer spacing of approximately 3.55 (Andersen et al.,2005). The (002) peak is accepted as representing the spacing between the layers of condensed aromatic structures. As reported in the literature, a single crystal graphite structure has interlayer spacing of 3.35, and amorphous carbon has an interlayer distance of 3.55 (Andersen et al., 2005; Trejo et al., 2007).

The value of d_M is related to the thickness and size of the aromatic sheets. Hence the interlayer distance for Canadian asphaltenes is in the range of amorphous materials of small order. The average distance between the saturated structures was calculated in similar manner by the relationship,

$$d_\gamma = \frac{5\lambda}{8\sin\theta} \tag{3.1}$$

The values of d_γ are calculated and reported in chapter 4. The average height of the asphaltene cluster, L_c was calculated by using the Scherrer crystallite size equation, which requires the determination of full width at half maximum (FWHM) of the graphene band.

$$L_c = 0.9\omega\cos\theta = \frac{0.45}{B[1/2]} \tag{3.2}$$

The values for L_c are reported in 4. The average number of aromatic sheets in a stacked cluster, M , is given by the values of L_c and d_M by using the equation,

$$M = \frac{L_c}{d_M} + 1 \tag{3.3}$$

The average layer diameter of the aromatic sheets, L_a can be calculated by the Scherrer crystallite size formula from the breadth $B[1/2]$ of the either the (100) or the (110) bands,

$$L_a = \frac{1.84\gamma}{\omega\cos\theta} = \frac{0.92}{B[1/2]} \tag{3.4}$$

The evaluation of the XRD-derived aromaticity f_a based on the gamma (γ) and (002) peak area. Aromaticity f_a, is the ratio of the carbon atoms present in aromatic rings to the total carbon atoms in the asphaltenes.

$$f_a = \frac{A_{(002)}}{(A_{(002)} + A_\gamma)} \tag{3.5}$$

where $A_{(002)}$ is the area under the (002) peak, A_γ is the area under the gamma (γ).

3.2   Sample Preparations

Asphalt binder samples were prepared as thin films on glass slide holders by heating to 150°C for about 10 minutes in a dry oven followed by removal and air cooling to room temperature.

3.2.1   Thin Film Method

There are several special considerations for using XRD to characterize thin film samples. High angular resolution is required because the peaks from semiconductor materials are sharp due to very low defect densities in the material. Consequently, multiple crystal monochromators are used to provide a highly collimated x-ray beam for these measurements. Prior to XRD each sample was placed on a glass slide and annealed in an oven at 150°C for 10 minutes in order to create a thin film of about 1mm thickness.

X-ray diffraction measurements were run on a Rigaku D/Max-2200V-PC using monochromatic Cu-K-α radiation operating at 40KV and 40mA. The range of scanning used is 5 to 110°2θ at a rate of $0.01°2\theta s^{-1}$ and count time of 5 s/step. The instrument is set up with a divergence slit of 0.5° and receiving slit of 0.3mm. Samples are analyzed before and after oxidation for 1 week at 20°. The full width at

half maximum (FWHM) and profile fits were obtained by using a Pearson VII and Pseudo-Voigt with fixed background over the ranges of 5 to $35°2\theta$ and 60 to $110°2\theta$. The x-ray pattern creation and analysis was performed using a Jade version 6.1 software package incorporating Pearson VII and Pseudo-Voigt functions. The collected data was normalized to a common background to compare spectra features from the four main peaks that we measured, ie γ, $(002)_{graphene}$, (100) and (110). All x-ray diffraction samples were prepared in aluminum sample holders, having test specimen dimensions of 25 mm diameter and 1 mm thickness.

Table 3.1 shows the specimen collected from specific location and some are unknown, however all the samples follow the PG standard set by CGSB.

3.2.2 Powder Method

Powder XRD is the most widely used x-ray diffraction technique for characterizing materials. As the name suggests, the sample is usually in a powdery form, consisting of fine grains of single crystalline material to be studied. The technique is used also widely for studying particles in liquid suspensions or polycrystalline solids or thin film materials. The term 'powder' really means that the crystalline domains are randomly oriented in the sample. Therefore when the 2-D diffraction pattern is recorded, it shows concentric rings of scattering peaks corresponding to the various d spacings in the crystal lattice. The positions and the intensities of the peaks are used for identifying the underlying structure of the material. For example, the diffraction lines of graphite would be different from diamond even though they both are made of carbon atoms. This phase identification is important because the material properties are highly dependent on structure (i.e. graphite and diamond).

A number of x-ray diffraction studies have investigated the powder diffraction

Asphalt Binders	Source	Modification Type	Grades
T1	western	Timmins, Ontario	PG 64-34
T2	Canadian unknown	RET + PPA oxidized	PG 64-34
T3	unknown	SBS	PG 64-34
T4	unknown	SBS + acid-modified	PG 64-34
T5	unknown	SBS	PG 64-34
T6	unknown	oxidized	PG 64-34
T7	unknown	acid-modified	PG 64-34
L1	Boundary Lake	Lamont, Alberta oxidized	80/100 A, PG 58-22
L2	Montana/Bow River	straight	150/200 B, PG 52-28
L3	Cold Lake	straight	300/400 A, PG 46-34
L4	Redwater	straight	80/100 C, PG 58-22
L5	Lloydminster	oxidized	80/100 A, PG 64-28
L6	Lloydminster	straight	150/200 A, PG 52-28
L7	Cold Lake	straight	200/300 A, PG 52-34
H1	Lloydminster	Hearst, Ontario straight	150/200 A, PG 52-33
H2	Venezuelan	straight	150/200 B, PG 52-33
N1	unknown	Northern Ontario straight	PG 52-34
N2	unknown	straight	PG 52-34
N3	unknown	acid-modified	PG 52-34
E9	unknown	acid-modified	PG 52-40
AAE	Lloydminster	Various Oxidized oxidized	60/70, PG 70-22
O1	unknown	oxidized	PG 58-34
O2	unknown	oxidized	PG 58-34

Table 3.1: Pertinent Asphalt Binder Properties.

Note: RET = reactive ethylene terpolymer; PPA = polyphosphoric acid; SBS = styrene-butadiene-styrene copolymer. Penetration grades are according to the Canadian Government Standards Board specification while PG grades are according to AASHTO M320.

pattern arising from asphaltenes chemically precipitated from asphalt cement in both original and laboratory aged samples. These investigators calculated the structural (aromaticity and crystallite) parameters found in the asphaltene powder samples to produce a cross-sectional model using collected x-ray diffraction data. As can be seen from the asphaltene cross-sectional model, the aromatic portions of the molecule tend to form stacks under the influence of London dispersion forces (also referred to as pi-stacking). Aliphatic side chains are represented within the asphaltene model extending from the central aromatic portion of the asphaltene molecule. These side chains are likely to be the template sites for wax crystallization.

In 2006, Lu and Redelius have isolated naturally occurring paraffin waxes from asphalt cement and investigated their x-ray diffraction spectra.

3.2.3 Spectral Line Shapes Modeled using Mathematical Functions

Separation of the γ and (002) bands in the above manner to determine aromaticity, f, involves three potential sources of error. Fortunately, in this study each of these could be dealt with in a reasonably satisfactory manner. The first of these possible errors arises from small angle scattering which tends to increase the intensity on the low angle side of the γ band. For broad peaks scattering is hard to detect due to there being no discrete lines, i.e. only decreasing intensity with increasing angle. Assuming an approximately symmetrical γ band, it was possible to attribute some of the intensity on the low angle side of the band to small angle scattering and hence to exclude it from the calculation of f. The second factor is that the intensity of a (002) band due to a seven layered unit of approximately 2.4nm thickness, for example, would exhibit an intensity 1.17 times that of the band for a two layered

unit of approximately 0.7-1.1 nm thickness. Thus, a variation in size distribution of the repeat units from sample to sample would result in an error in f. Fortunately, the asphalt binders under study have about the same L, and FWHM of the γ band, indicating a similar size distribution.

3.2.4   Pearson VII and Pseudo-Voigt

Diffraction is done using much different tools than decades ago both regarding instrumentation and especially data analysis. Numerous computer programs give solutions for almost any task, and the amount of information obtainable from a simple powder-diffraction scan is astonishing. Hence, it is likely that line-broadening analysis will become a part of routine program output, together with line positions, intensities, lattice parameters, etc. Full pattern analysis software, such as in some retrieved refinement programs, already includes refinable parameters corresponding to domain size and strain. Unfortunately, inspection of line broadening is rarely a standard procedure. Being so automated, line-broadening analysis is very often inaccurate because of inadequate models used in most retrieved programs. Instead, the approach based on a Voicing function (Balzac and Led better 1995), which is generally applicable and probably much more accurate than current models, may be more useful.

During decades of research, it became more and more obvious that neither Cauchy nor Gauss functions can adequately model diffraction line broadening. Here it was shown that a model based on a Voigt function may be more realistic and accurate. Moreover, previously considered as divergent approaches, namely the Warren-Averbach analysis and the integral-breadth methods, are consistently related. Some common occurrences in Warren-Averbach analysis, particularly the "hook" effect, functional dependence of mean square strain on averaging distance, and ratio of

volume-weighted to the surface weighted domain size, all follow from the "double-Voigt" model. Some possible limitations of Voigt-based models are both of conceptual (asymmetric physically broadened profiles) and practical (observed line profiles may fall below the Voigt-Cauchian limit) nature. Without a better function of choice in the future, the Voigt function may still prove to be a satisfactory approximation in most cases.

The Voigt functional form has been the basis for most quantitative analysis of x-ray photoelectrons spectroscopy (XPS) spectra. Unfortunately, an analytic form for the convolution of a Gaussian with a Lorentzian ($G * L$) is not available and so practical systems have adopted two approximations to the true Voigt function. Gaussian or Lorentzian Product Form:

$$GL(x, F, E, m) = \frac{\exp(-4ln2(1 - m)\frac{(x-E)^2}{F^2})}{(1 + 4m\frac{(x-E)^2}{F^2}}$$
(3.6)

Gaussian or Lorentzian Sum Form:

$$SGL(x, F, E, m) = (1 - m)\exp(-4ln2(1 - m)\frac{(x - E)^2}{F^2}) + \frac{m}{(1 + 4\frac{(x-E)^2}{F^2}}$$
(3.7)

3.3 Exponential Asymmetric Blend Based upon Voigt-type Line-Shapes

Given either of the above Gaussian or Lorentzian symmetric line-shapes, an asymmetric profile is obtained from a blend function as follows,

$$Y(x) = GL(x) + (1 - GL(x)) * T(x)$$
(3.8)

Where,

$$T(x, k, F, E) = \begin{cases} \exp(-k\frac{(x-E)}{F}) & \text{if } x \leq E \\ 1 & \text{Otherwise} \end{cases}$$

3.4 Line Shapes Analysis Using Peak Search and Profile Fit

The XRD spectra were peak searched using a parabolic filter (10,000 raw data points, screened out Kα-2 peaks, peak location summit, threshold sigma 3.0, intensity cutoff 0.1 percent, range to find background 1.0, points to average background 7) over the angular range of 5° to 110°. The full width at half maximum (FWHM) and profile fits were obtained by using either Pearson VII and pseudo-Voigt function (fixed background, exponent = 1.5 and Lorentzian = 0.5) over the ranges 5° to 35° 2θ and 60° to 110° 2θ on the XRD line spectra of interest. The XRD spectra were also modeled in Mathematica using a generalized Fermi function (GFF).

3.5 Generalized Fermi Function

Generalized Fermi function (Eq. 4.6) has been used in Mathematica software and employed to fit raw data from XRD on the Generalized Fermi function. Some of the procedures and code followed during computation and simulation of specimens are shown in the Appendix.

Chapter 4

Results and Discussion

These XRD patterns consist of the four major peaks in asphaltene binders (γ, $(002)_{graphene}$, (100), (110)) as describe in the Yen model. In addition to these peaks, there are peaks present in some samples (E9, L1, L4) due to additional chemical phases such as paraffins, wax. and other impurities.

From Table 4.1 the data indicates GFF values range from $f_a = 0.08$ to 2.40 and $d_M = 3.95$ to 17.40. This indicates that the profile fitting in GFF is less consistent than that for P and V, due to the asymmetry of the XRD patterns. Therefore, GFF is more sensitive to asymmetry and results in higher and lower values of aromaticity (f_a) and crystallite parameters (d_M).

4.1   XRD Patterns

The XRD patterns created for the 23 different asphalt binder samples were generated by standard methods as described in the experimental and Jade software. Figures 4.1 to 4.8 represent 15 of the 23 asphalt binders (N1, to N3, L1 to L7, E9, H1, H2, O1, O2) as shown below.
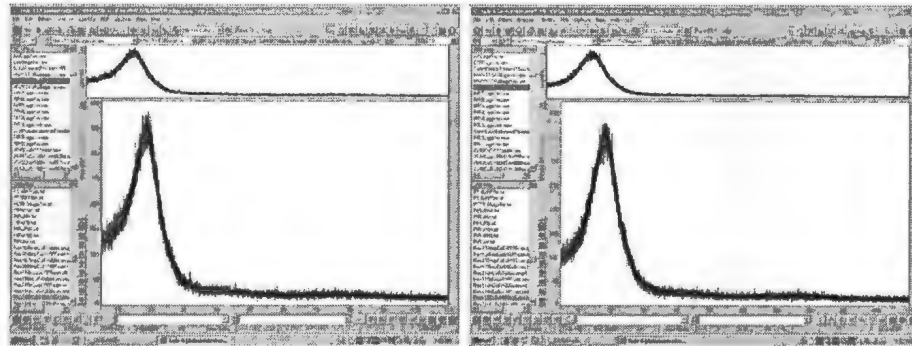
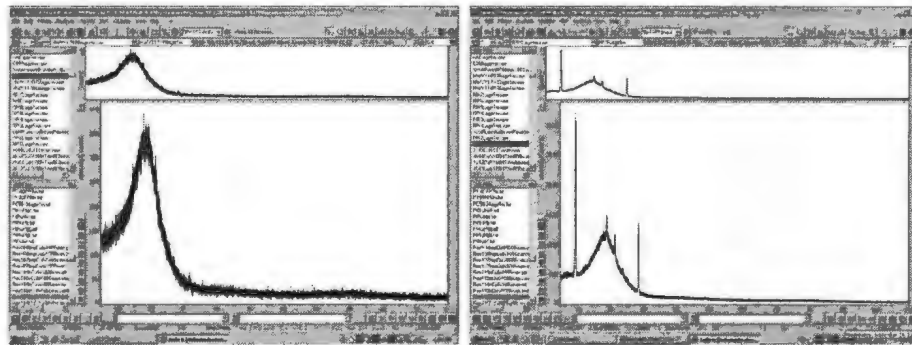Figure 4.1: Specimen N1 and N2 of XRD profile.

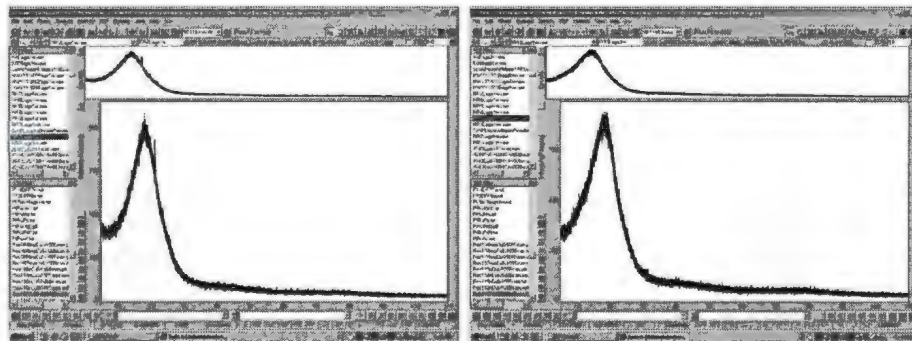Figure 4.2: Specimen N3 and L1 of XRD profile.

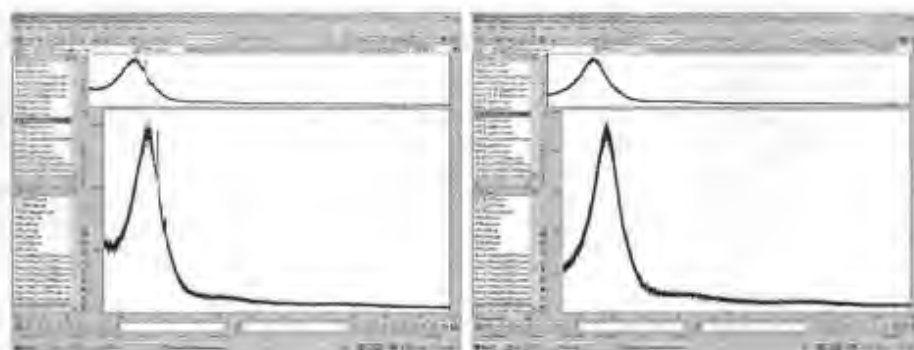Figure 4.3: Specimen L2 and L3 of XRD profile.

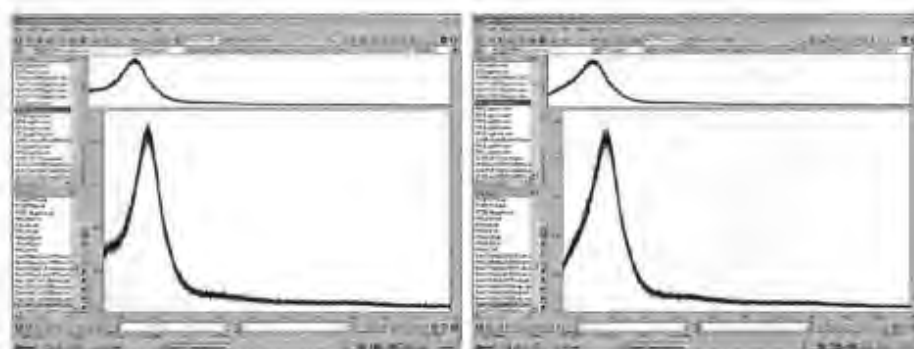Figure 4.4: Specimen L4 and L5 of XRD profile.

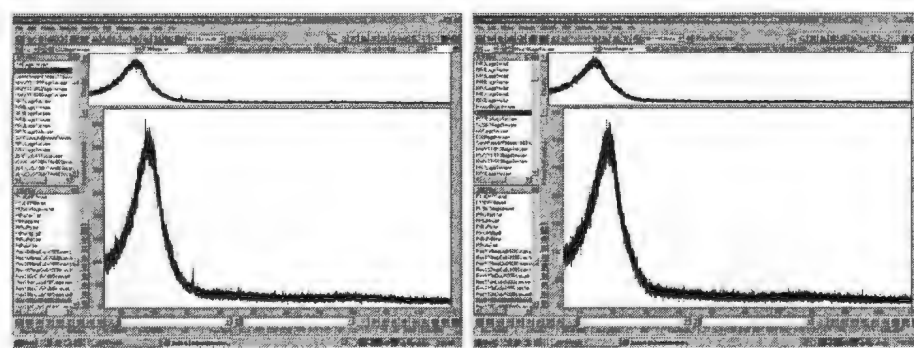Figure 4.5: Specimen L6 and L7 of XRD profile.

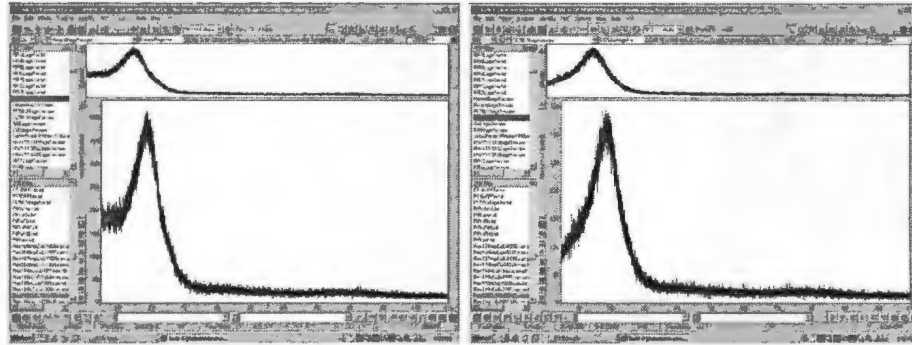Figure 4.6: Specimen E9 and H1 of XRD profile.

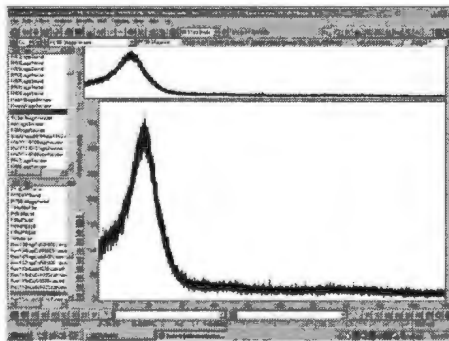Figure 4.7: Specimen H2 and O1 of XRD profile.

Figure 4.8: Specimen O2 of XRD profile.

4.2 XRD Measurements and Calculations

The XRD data were fit with either a profile function that is a pseudo-Voigt or Pearson VII (see Figure 4.9). Pseudo-Voigt is a linear combination of Gaussian and Lorentzian components and a true Voigt is a convolution of the Gaussian and Lorentzian components; but this function is more difficult to implement computationally. This leaves Pearson VII which is an exponential mixing of Gaussian and Lorentzian components. The shapes, symmetry and application of Pseudo-Voigt and Pearson VII will be described further in the next section.
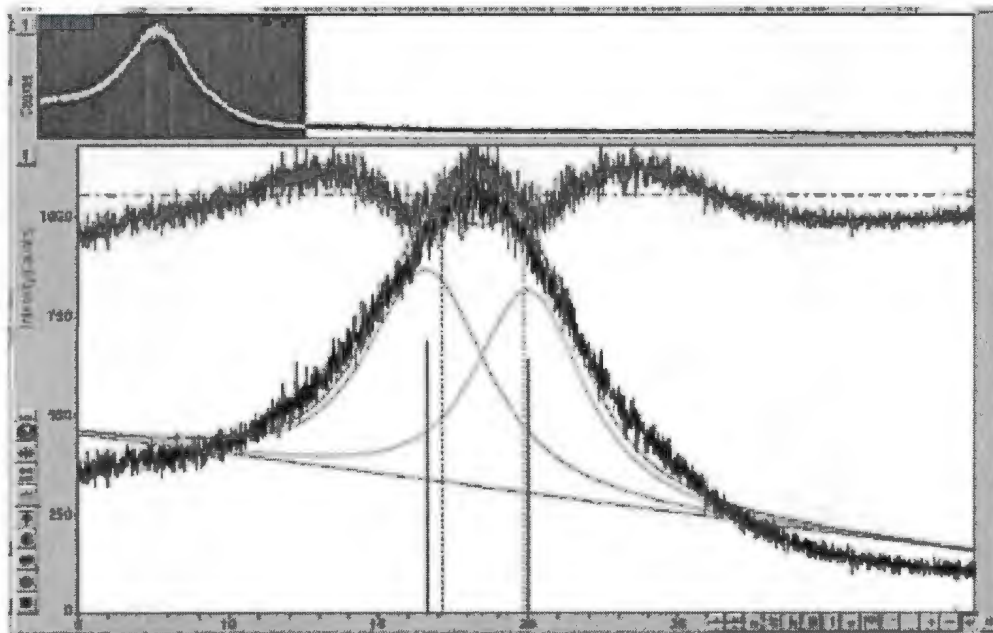

Figure 4.9: XRD profile fit of asphalt binders

4.3 Peak Shape Functions

Considering (Figures 4.1 to 4.8) the intensity, $Y(i)$, of the ith point ($1 \leq i \leq n$, where n is the total number of measured points) of the diffraction pattern, in the most general form is the sum of the contributions, y_k, from the m overlapped individual Bragg peaks ($1 \leq k \leq m$) and the background, $b(i)$.

$$Y(i) = b(i) + \sum_{k=1}^{m} I_k[y_k(x_k) + 0.5y_k(x_k + \Delta x_k)] \qquad (4.1)$$

where:

I_k is the intensity of the kth Bragg reflection, $x_k = 2\theta_i - 2\theta_k$ and Δx_k is the difference between the Bragg angles of the $K\alpha_2$ and $K\alpha_1$ components in the XRD doublet γ, graphene(002) in asphalt binders. The presence of Bragg intensity as a multiplier in the above equation enables one to introduce and analyze the behavior of different normalized functions independently of peak intensity, i.e. assuming that the definite integral of a peak shape function, calculated from negative to positive infinity, is unity in each case. The four most commonly used empirical peak shape functions (y) are as follows,

Gauss:

$$y(x) = G(x) \quad = \quad \frac{C_G^{1/2}}{\sqrt{\pi}H} \exp\left(-C_G x^2\right) \qquad (4.2)$$

Lorentz:

$$y(x) = L(x) \quad = \quad \frac{C_L^{1/2}}{\pi H'}(1 + C_L x^2)^{-1} \qquad (4.3)$$

Pseudo-Voigt (Linear combination of Gaussian and Lorentizian)

$$y(x) = PV(x) \quad = \quad \eta \frac{C_G^{1/2}}{\sqrt{\pi}H} \exp\left(-C_G x^2\right) + (1 - \eta)\frac{C_L^{1/2}}{\pi H'}(1 + C_L x^2)^{-1} \quad (4.4)$$

Pearson-VII:

$$y(x) = PVII(x) \quad = \quad \frac{\Gamma(\beta)}{\Gamma(\beta - 1/2)}\frac{C_P^{1/2}}{\sqrt{\pi}H}(1 + C_P x^2)^{-\beta} \quad (4.5)$$

GFF:

$$h(s) \quad = \quad \frac{A}{\exp\left(-a(s - c)\right) + \exp\left(b(s - c)\right)} \quad (4.6)$$

where A, a, b, c are unknown parameters to be input and s $= \frac{2\sin(\theta)}{\lambda}$ while the values A and c describe the amplitude and the position of the fit, a and b control shape of the fit.

H and H', are the full widths at the half maximum (FWHM).

$$x = \frac{(2\theta_i - 2\theta_k)}{H_k}, \quad (4.7)$$

is essentially the Bragg angle of the ith point in the diffraction pattern with its origin in the position of the kth peak divided by the peak's FWHM.

$2\theta_i$, is the Bragg angle of the ith point of the diffraction pattern.

$2\theta_k$, is the calculated (or ideal) Bragg angle of the kth Bragg reflection.

$C_G = 4\ln2$, and $\frac{C_G^{1/2}}{\sqrt{\pi}H}$, is the normalization factor for the Gauss function such that,

$$\int_{-\infty}^{\infty} \frac{C_G^{1/2}}{\sqrt{\pi}H} \exp\left(-C_G x^2\right) dx = 1 \qquad (4.8)$$

$C_L = 4$, and $\frac{C_L^{1/2}}{\pi H'}$, is the normalization factor for the Lorentz function such that,

$$\int_{-\infty}^{\infty} \frac{C_L^{1/2}}{\pi H'}(1 + C_L x^2)^{-1} dx = 1 \qquad (4.9)$$

$C_P = 4(2^{1/\beta} - 1)$, and $\left[\frac{\Gamma(\beta)}{\Gamma(\beta-1/2)}\right]\frac{C_P^{1/2}}{\sqrt{\pi}H}$

is the normalization factor for the Pearson-VII function such that,

$$\int_{-\infty}^{\infty} \frac{\Gamma(\beta)}{\Gamma(\beta - 1/2)} \frac{C_P^{1/2}}{\sqrt{\pi}H}(1 + C_P x^2)^{-\beta} dx = 1 \qquad (4.10)$$

$$H = (U\tan^2\theta + V\tan\theta + W)^{1/2}, \qquad (4.11)$$

which is known as Caglioti formula. It is the FWHM as a function of θ for Gauss, Pseudo-Voigt and Pearson-VII functions, and U, V and W are free variables. (Pecharsky et al., 2005).

$$H' = \frac{U}{\cos\theta} + V\tan\theta, \qquad (4.12)$$

is the FWHM as a function of θ for the Lorentz function, and U and V are free variables.

$$\eta \;=\; \eta_0 + \eta_1 2\theta + \eta_2 \theta^2 \tag{4.13}$$

where, $0 \leq \eta \leq 1$, and η is the Pseudo-Voigt function mixing parameter, i.e. the fractional contribution of the Gauss function into the linear combination of Gauss and Lorentz functions, η_0, η_1 and η_2 are free variables whereas, Γ, is the gamma function.

$$\beta = \beta_0 + \frac{\beta_1}{2\theta} + \frac{\beta_2}{(2\theta)^2} \tag{4.14}$$

β is the exponent as a function of Bragg angle in the Pearson-VII function, and β_0, β_1 and β_2 are free variables.

The illustration of Gauss (dashed-dotted line) and Lorentz (solid line) peak shape functions and the FWHM are shown as thick horizontal arrows (see figure 4.10). The two simplest peak shape functions represent Gaussian and Lorentzian distributions, respectively, of the intensity in the Bragg peak. From the figure the Lorentz function is sharp near its maximum but has long tails on each side near its base. The Gauss function has no tails at the base but a round maximum. Both functions are centrosymmetric, i.e., $G(x) = G(-x)$ and $L(x) = L(-x)$.

The shapes of real Bragg peaks, which are the results of convoluting multiple instrumental and specimen functions are rarely described well in XRD by simple Gaussian or Lorentzian distributions, especially in x-ray diffraction. Usually experimental peak shapes are located somewhere between the Gauss and Lorentz distributions and they can be better represented as the mixture of the two functions. One way would be to convolute the Gauss and Lorentz functions in different proportions. This convolution, somewhat of a complex procedure, that requires numerical integration
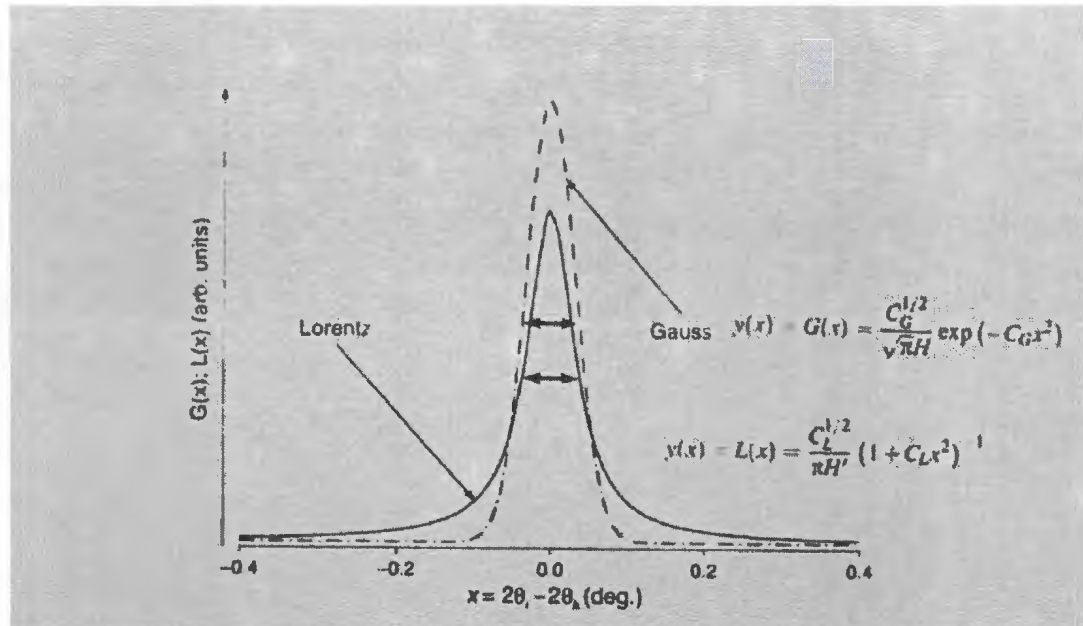
Figure 4.10: Gauss and Lorentz peak shape functions (Pecharsky et al., 2008).

when one or several peak shape function parameters change. Therefore, instead of a convolution, a much simpler linear combination of Gauss and Lorentz functions (Pseudo-Voigt) is used instead of a convolution. The Gaussian and Lorentzian compounds are mixed in η to 1-η ratio, so that the value of the mixing parameter, η, varies from 0 Lorentz to 1 Gauss. However, η is not meaningful outside this range. The other used peak shape function is Pearson-VII (Eq.4.5).

It is similar to Lorentz distribution except that the exponent (β) varies in the Pearson-VII, while it remains constant ($\beta = 1$) in the Lorentz function. Pearson-VII, provides an intensity distribution close to the Pseudo-Voigt function: when the exponent, $\beta = 1$, it is identical to the Lorentz distribution, and when $\beta \cong 10$, Pearson-VII becomes equal to of Gaussian function.

Thus, when the exponent is in the range $0.5 < \beta < 1$ or $\beta > 10$, the peak shape extends beyond Lorentz or Gauss functions, respectively, but values of β are seldom

observed in practice. An example of the x-ray diffraction profile fitting using Pearson-VII function is shown in the figure below. Both the Pseudo-Voigt and Pearson-VII functions are symmetric. The argument, x, in each of the four empirical functions above establishes the location of peak maximum, which is obviously observed when

$x = 0$ and $2\theta_i = 2\theta_k$.

For pseudo-Voigt and Pearson VII functions:

-Peak shape is modeled using the pseudo-Voigt or Pearson VII functions.

-The FWHM term, H, is a component of both functions.

-The FWHM is correlated to crystallite size and microstrain.

-The FWHM is modeled using the Cagliotti Equation (Eq.4.11).

-U is the parameter most strongly associated with strain broadening.

-Crystallite size can be calculated from U and W.

-U can be separated into (hkl) dependent components for anisotropic broadening.

Hence, in the most general case the peak FWHM at a specific 2θ angle is represented as,

$$FWHM = H = \sqrt{U \tan^2 \theta + V \tan \theta + W} \qquad (4.15)$$

A second parameter, determining the value of the argument, is the FWHM, H. The later varies with 2θ and its dependence on the Bragg angle is most commonly represented by an empirical peak broadening function, which has three free parameters U, V, and W (except for the Lorentzian, which usually has only two free variables).

4.4   Spectral Line Shapes Analysis

Profile fits of XRD (PVII and Psudo-Voigt) and GFF simulation results. The re-mained results can be seen in the Appendix.

4.4.1   Sample figures after simulation with GFF

The following figures corresponding to 5 of the 23 samples (H1, O1, O2, L3, and T5) of the GFF profile fits from XRD data are shown below. The four bands (peaks) in the figures represent the γ, $(002)_{graphene}$, (100), and (110) are the same as found in the XRD patterns. Additional data for the rest of the samples can be found in the appendix.
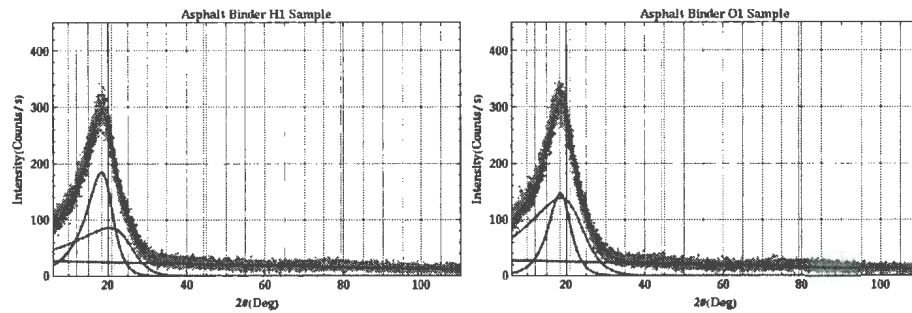

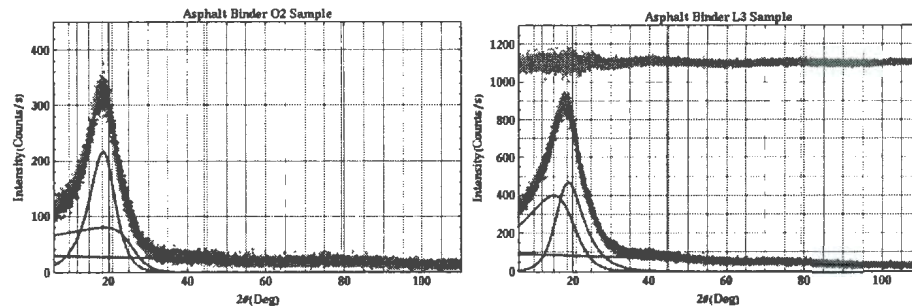Figure 4.11: Samples H1 and O1 from GFF.

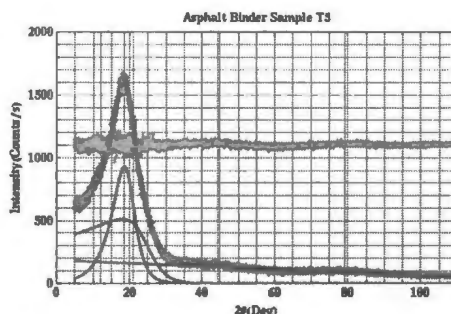Figure 4.12: Samples O2 and L3 from GFF.

Figure 4.13: Sample T5 from GFF.

4.5   Comparing the Results of all Asphalt Samples

The x-ray diffraction patterns observed requires fitting of the theoretical distributions which is crucial in order to get information from the spectral lines. Pearson-VII and Pseudo-Voigt fitting procedures are used and the three major bands γ, (002), and (100) positioned at approximately $2\theta = 20°$, $25°$, and $44°$ were used as the initial estimates. On the high 2θ side of the (100) peak, the (004) band may be observed in some cases at 2θ at approximately around $53°$. Also, estimates of the peak width and intensity were needed to initiate the regression. Backgrounds are a major issue in the x-ray diffraction patterns of asphaltene as observed in this work and they were set as linear.

On the low 2θ side, the baseline is not sufficiently well defined, so one must use the high value end of the x-ray diffraction pattern and fix this as a constant baseline. This introduces the potential for a reasonable assumption, inspired guesswork, or statistical inaccuracies that may influence the outcome in favor of the operator. The change in baseline, however, had in most cases very little influence on the relative results such as the aromaticity. In all cases manual refinements were added to enhance regression coefficients. But, this compromises the change of peak position as well as width, leading to, as yet, a real but indeterminate degree of operator bias involved

that does, indeed, affect the results.

Table 4.1 contains the aromaticity and crystallite parameters calculated using Pearson VII, Pseudo-Voigt and GFF shown below.

	f_a			$d_M(A°)$			$d_\gamma(A°)$			$L_a(A°)$			$L_c(A°)$			M_c		
Sample	P	V	GFF	P	V	GFF	P	V	GFF	P	V	GFF	P	V	GFF	P	V	GFF
L1	0.53	0.53	0.943	4.4	4.4	17.4	6.5	6.6	5.99	3.4	3.4	3.54	6.6	5.9	6.45	2.5	2.3	1.4
L2	0.44	0.47	0.313	4.4	4.4	4.23	6.7	6.7	6.08	4.9	4.9	3.29	6.3	6.8	5.73	2.4	2.5	2.4
L3	0.51	0.55	0.619	4.5	4.5	4.7	7.0	7.1	5.84	5.6	5.6	3.10	6.0	5.4	5.73	2.3	2.2	2.22
L4	0.40	0.46	0.32	4.4	4.4	4.75	6.6	6.7	5.99	4.9	4.9	3.01	6.9	6.1	6.45	2.6	2.4	2.35
L5	0.46	0.55	2.40	4.4	4.5	4.65	6.8	7.0	5.96	5.3	5.3	3.59	5.4	4.7	6.45	2.2	2.0	2.40
L6	0.47	0.50	0.363	4.4	4.4	4.79	6.7	6.7	5.78	4.5	4.5	3.42	6.2	5.6	6.62	2.4	2.3	2.38
L7	0.59	0.72	0.969	4.6	4.7	3.95	7.5	8.0	5.99	4.7	4.7	3.59	4.2	3.6	5.16	1.9	1.8	2.30
N1	0.50	0.52	0.61	4.5	4.5	17.67	6.8	6.9	5.92	4.3	4.3	3.25	6.8	6.2	4.69	2.5	2.4	1.94
N2	0.48	0.50	0.705	4.5	4.5	5.37	6.6	6.7	5.99	4.0	4.0	3.25	7.9	7.3	5.48	2.8	2.6	2.02
N3	0.46	0.47	0.50	4.4	4.4	5.04	6.6	6.6	5.96	3.9	3.9	3.51	8.3	7.7	5.26	2.9	2.8	2.04
E9	0.52	0.54	0.62	4.5	4.5	5.06	6.8	6.9	5.99	3.4	3.4	3.45	6.6	6.1	5.06	2.5	2.4	2.00
AAE	0.51	0.52	0.792	4.3	4.3	4.82	6.5	6.6	5.93	4.5	4.5	3.61	6.2	5.7	5.61	2.4	2.3	2.16
O1	0.48	0.51	0.312	4.4	4.4	4.67	6.7	6.7	5.84	3.2	3.2	4.84	7.0	6.4	5.37	2.6	2.5	2.15
O2	0.47	0.50	0.511	4.4	4.4	4.79	6.7	6.7	5.99	4.2	4.2	3.54	7.4	6.7	5.16	2.7	2.5	2.08
H1	0.52	0.56	0.529	4.5	4.5	4.39	6.9	7.0	6.08	4.9	4.9	3.49	6.6	6.0	5.26	2.5	2.3	2.19
H2	0.43	0.48	0.55	4.4	4.4	5.01	6.5	6.6	5.91	5.0	5.0	3.59	7.6	5.7	5.16	2.7	2.3	2.03
T1	0.45	0.54	0.52	4.4	4.4	4.78	6.5	6.7	5.91	3.3	3.3	3.51	5.5	4.7	4.69	2.3	2.1	1.98
T2	0.53	0.66	0.582	4.5	4.5	4.77	6.9	7.3	6.00	3.7	3.7	3.77	5.2	4.4	5.17	2.2	2.0	2.08
T3	0.53	0.60	0.521	4.51	4.5	4.19	7.0	7.2	5.99	3.3	3.3	3.30	5.3	4.6	4.69	2.2	2.0	2.12
T4	0.55	0.69	0.553	4.5	4.6	4.67	7.0	7.4	6.25	3.2	3.2	3.29	5.2	4.4	4.69	2.2	2.0	2.00
T5	0.49	0.57	0.591	4.5	4.5	4.80	6.9	7.1	5.66	3.4	3.4	3.29	6.2	5.4	5.73	2.4	2.2	2.19
T6	0.65	0.73	0.080	4.6	4.6	7.14	7.6	8.0	5.99	3.1	3.1	3.29	4.4	3.9	4.30	2.0	1.8	1.60
T7	0.52	0.53	0.284	4.5	4.5	5.23	6.9	6.9	5.93	3.3	3.3	3.10	5.9	6.3	5.17	2.3	2.4	1.98

Table 4.1: Aromaticity and crystallite parameters calculated using Pearson VII, Pseudo-Voigt and GFF.

Aromaticity (f_a) of approximately values 0.08 for T6 and 2.40 for L5 using GFF shows that the data fits were found to be very poor. For instance, asphaltene T6 does look, from the appearance of the XRD profile, as apparently having a large

(002) contribution. However, when using GFF the γ peak becomes very broad and hence the (002) contribution becomes very small, making the aromaticity in the range of only 0.08, while the Pearson VII and Pseudo-Voigt give consistent aromaticity of approximately 0.65 and 0.73 respectively. The same is seen for asphaltene T7, having an f_a of about 0.284 when fitted in GFF and 0.52 and 0.53 are obtained using the same procedure Pearson VII and Pseudo-Voigt functions. On the other hand, samples L1 and L7 have an apparent f_a of about 0.943 and 0.969 from GFF which are relatively high but about similar values from both Pearson VII and Pseudo-Voigt calculation for both samples. The higher aromaticity values for L1 and L7 indicates that a very distorted x-ray diffraction pattern at low angles that has a strong impact on the quality of the fit. For the rest of the samples, attempts at fitting an individual peak gave an aromaticity with approximately similar results with an error of ± 0.1.

The crystallite parameter of the interlayer distance d_M has extremely higher values of 17.4 and 17.67 from GFF compared to Person VII and Pseudo-Voigt. However, the rest of the results for all other samples are consistent.
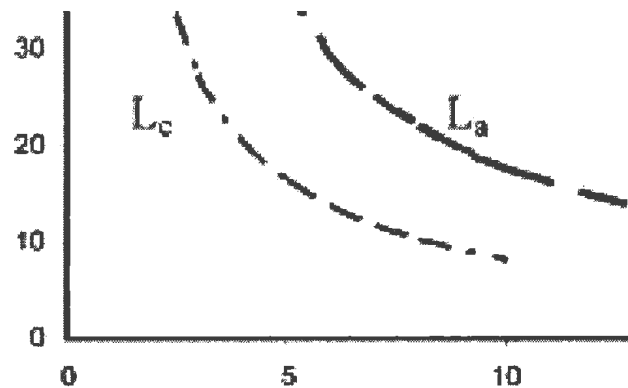
Figure 4.14: Modified figure of relationship showing crystalline dimension (vertical) versus bandwidth (horizontal) (Anderson et al., 2005).

The two crucial parameters to understand crystallite size are L_c and L_a. These

parameters are very sensitive to FWHM, as observed in (Figure 4.14), where a theoretical relation between L_c and L_a has been calculated. It is evident that L_c is sensitive to small changes in γ, i.e., a change from $2\theta = 5°$ to $6°$ causes the stack height to decrease from 3.0 to 1.5nm. The sheet diameter data are less sensitive and remain almost constant around 1.1 to 1.5nm, and only for the narrow (100) band will an effect be important. Again, we observe that the basic results are very different also in terms of trends when changing from Pearson VII to Pseudo-Voigt in XRD. The fitting procedure may indeed be oversimplified in that graphing normally involve a formation of non symmetric (002) peaks formed by several contributions, such as noise in the residue of the data.

Chapter 5

Conclusions

Comparison of XRD pattern profile fits by Pearson VII and Pseudo-Voigt were directly compared to measure aromaticity and crystallite parameters with higher and lower values often observed. A generalized Fermi function was used to model the XRD data in mathematica with mixed results relative to Pearson VII and Pseudo-Voigt functions. The results can be explained in terms of peak shape functions, profile fitting, and assymetry of XRD data.

Twenty three asphaltene samples were prepared from different sources and analyzed by XRD (Pearson VII and Pseudo-Voigt) as raw data, and by GFF modeling. From zero to seven days (one week), the aging process for all asphalt binders increased. As time elapses, the peaks were marked and analyzed. Thus, we observe that, the crystallinity is increasing with increasing exposure of asphalt binder with aging. A minute change in the angles of the profiles shows that a change of planes of the atoms. The results showed a correlation among Pearson VII, Pseudo-Voigt and GFF.

XRD experiments unveiled some features of asphaltene aggregates. The cluster of associated asphaltene molecules with stacked aromatic sheets are relatively stable up

to 150°C, and the layer distance between aromatic sheets and the number of aromatic sheets in a stacking cluster are uniform in three asphaltene species.

Future analyses will search the relation among variation of values intensities with the variation of the chemical components in the material because the aging is generally associated with oxidation at the molecular level. Analysis of the results obtained in this work indicates that the x-ray diffraction provides insight on understanding the structural and compositional properties of asphalt binders, which is significant in understanding of the aging of asphalt binders and pavement.

X-ray diffraction (XRD) results compliment the civil engineering tests as reported by most research studies, but it is unreasonable to expect the XRD results to strongly predict the major cosequences of issues such as performance and durability of asphalt pavement. Further testing is required to confirm these issues and then this would become a PhD scope of work.

Chapter 6

Recommendations for Future Work

As the challenges elevates to extract materials in their purest form, such as asphaltene, a new way of designing techniques should be implemented to improve the productivity and durability of materials.

Develop mix designs for high-modulus asphalt mixes, including the selection of binder, optimum asphalt content for low voids, and required stiffness.

Develop an understanding of pavement layer bonding. From both a construction and a performance standpoint, it is crucial to understand how bonding occurs between pavement layers and its role in pavement responses to loads, by studying the structure and composition of the mix samples at microscopic level.

Bibliography

[1] Airey, G.D., Rheological Properties of Styrene Butadiene Styrene Modified Road Bitumens, Fuel, 82(2003)1709-1719.

[2] Akbarzadeh, K., Hammami, A., Kharrat, A., Zhang, D., Allenson, S., Creek, J., Kabir, S., Jamaluddin, A., Marshall, A.G., Rodgers, R.P., Mullins, O.C. and Solbakken, T., Asphaltenes-Problematic but Rich in Potential. Oilfield Review, 19(2007)22-43.

[3] Aldea N.,Tiusan C.V. and Barz B., A New X-ray Line Profile Approximation Used For the Evaluation of the Global Nanostructure of Nickel Clusters, Journal of Optoelectronics and Advanced Materials, 6(2004)225-235.

[4] Ali, L.H., A method for the calculation of molecular weights of aromatic compounds, and its application to petroleum fractions, Fuel, 50(1971)298.

[5] Altamirano, J.J., Flores, M.A., Pie, O., Panivino, N., Arzate, C., Kappellmann, G., Lopez, M.T., Espinosa, S., Rosales, S., Characterization Fisico-quimica de Asphaltenos Procedents de los Crudos Maya e Istmo, Revisita del Instituto Mexico del Petroleo, 18(1986)32-44.

[6] Andersen, S.I., Jensen, J.O. and Speight, J.G., X-ray Diffraction of Subfractions of Petroleum Asphaltenes, Energy and Fuels, 19(2005)2371-2377.

85

[7] Atsushi, T., Hiroshi N., Daishiro I.and Yoshiro O., Structure Determination of Altemicidin by n.m.r. Spectroscopic Analysis, 47(1991)3621-3632. (replace for Doddrle)

[8] Bahia, H.U., Anderson, D.A. and Christensen, D., The Bending Beam Rheometer: A Simple Device for Measuring Low Temperature Rheology of Asphalt Binders, Journal of the Association of Asphalt Paving Technologists, 62(1993)93-129.

[9] Bayat, M., Sattarin, M. and Teymouri, M., Prediction of Asphaltene Self-Precipitation in Dead Crude Oil, Energy and Fuels, 22(2008)583-586.

[10] Bell, Summary Report On Aging Of Asphalt Aggregate Systems, Transportation Research Board, 1989.

[11] Bouquet, M. and Bailleul, A., Application to Every Kind of Petroleum Fractions Including Residues and Asphaltenes, Fuel, 65(1986)1240.

[12] Brown, Proceedings of the Association of Asphalt Paving Technologists, 27(1958)171-176.

[13] Boussingault M., Memoire sur la Composition des Bitumes, Annales de Chimie et de Physique, Vol.LXIV, (1937)141-151.

[14] Choquet, F.S., and Verhasselt, A.F., Proceedings of Strategic Highway Research Program (SHRP) and Traffic Safety on Two Continents, Hague, (1994)193-213.

[15] Christensen W.D. and Bonaquist R., Use of Strength Tests for Evaluating the Rut Resistance of Asphalt Concrete, Asphalt Paving Technology, Association of Asphalt Paving Technologists-Proceedings of the Technical Sessions, 71(2002)692-711.

[16] Christopher,J., Amarjeet, S.S., Gurpreet, S.K., Agadi, K., Babu, R.T., Mukesh, C.J., Surendra, K.J., Akhilesh, K.B., Chemical Structure of Bitumen-derived Asphaltenes by Nuclear Magnetic Resonance Spectroscopy and X-ray Diffractometry, Fuel, 75(1996)999-1008.

[17] Christy, A.A., Dahl, B. and Kvalheim, O.M., Structural Features of Resins, Aspaltenes and Kerogen Studied by Diffuse Reflectance Infrared Spectroscopy, Fuel, 68(1989)430.

[18] Chuck, M., James R.S., Development of Performance Grade Binder Selection Method for Canadian Airport Pavements, The Federal Aviation Adminstration Technology Transfer Conference, 1999.

[19] Clutter, D.R., Petrabes, L., Stenger, R.L. and Sensen, R.K., Nuclear Magnetic Resonance Spectrometry of Petroleum Fractions, Carbon-13 and Proton Nuclear Magnetic Resonance Characterizations in Terms of Average Molecule Parameters, Analytic Chemistry, 44(1972)1395-1405.

[20] Decroocq, D., Thomas, M., Fixari, B., Le Perchec, P., Bogois, M., Lena, L., Des Couriers, T. and Rossarie, Improving Heat Treatment Processes for Residues by Optimizing the Transformation of Resins and Asphaltenes, Oil and Gas Science and Technology, 47(1992)103-131.

[21] Dereppe, J.M., Moreaux, C. and Cartex, H., Analysis of Asphaltenes by Carbon and Proton Nuclear Magnetic Resonance Spectroscopy, Fuel, 57(1978)435.

[22] Dickenson, E.M., Average Structures of Petroleum Pitch Fractions by HCn.m.r. Spectroscopy, Fuel, 64(1985)704-706.

[23] Dickie, J.P. and Yen, T.F., Macrostructures of Asphaltic Fractions by Various Instrumental Methods, Analytic Chemistry, 39(1967)1847-1852.

[24] Dow, Proceedings of the ASTM 6th Annual Meeting, Delaware, 3(1903)349-373.

[25] Ebert, L.B., Scanlon, J.C. and Mills, D.R., X-ray diffraction of n-paraffins and stacked aromatic molecules: Problems in Using Diffraction to Determine The structure of Asphaltene, Am. Chem. Soc. Div. Pet. Chem. Preprints, 28(1983)1353.

[26] Ergun, S., Tiensuu, V.H., Interpretation of the Intensities of X-Rays Scattered by Coals, Fuel, 38(1959)64-78.

[27] Galal K.A., and White T.D., Correlations Between Superpave Asphalt Stiffness and In-Service Pavement Performance, 80th Annual Meeting of the Transportation Research Board, Washington, D.C., 2001.

[28] G-Source: http://www.guides-gallois.com, World Highways, Asphalt Review, 25(2)(2006).

[29] Gawel and K. Baqinska, Effect of Chemical Nature on The Susceptibility of Asphalt to Aging, Petroleum Science and Technology 22(2004)1261-1271.

[30] Gavel, I., Fuel, 66(1987)618.

[31] Giavarni, C. and Vecchi, C., In 'IVth Europbitumen Symposium, (1989)261.

[32] Gordon D.A., Rheological evaluation of ethylene vinyl acetate polymer modified bitumens, Construction and Building Materials, 16(2002)473-487.

[33] Goual L., Sedghi M., Zeng H., Mostowfi F., McFarlane R., and Mullins O.C., On the Formation and Properties of Asphaltene Nanoaggregates and Clusters by DCConductivity and Centrifugation, Fuel, 90(2011)2480-2490.

[34] Groenzin, H. and Mullins, O.C., Asphaltene Molecular Size and Structure, Journal of Physical Chemistry A, 103(1999)11237-11245.

[35] Groenzin, H. and Mullins, O. C., Molecular Size and Structure of Asphaltenes from Various Sources, Energy Fuels, 14(2000)677-684.

[36] Harrison, I.R., Wang, G. and Hso,T.C., A Differential Scanning Calorimetry Study of Asphalt Binders, Strategic Highway Research Program report No. A/UFR-92-612, National Research Council, Washington, DC., 1992.

[37] Harvey J.T., Deacon J.A., Tsai B.W., and Monismith C.L., Fatigue Performance of Asphalt Concrete Mixes and Its Relationship to Asphalt Concrete Pavement Performance in California, Asphalt Research Program: CAL/APT Program, Institute of Transportation Studies, University of California, Berkeley, 1995.

[38] Herzog, P., Tchoubar, D. and Espinat, D., Macrostructure of Asphaltene Dispersions by Small Angle X-ray Scattering, Fuel, 67(1988)245.

[39] Hesp, S.A.M., Illiuta, S. and Shirokoff, J., Reversible Aging in Asphalt Binders, Energy and Fuels, 21(2007)1112-1121.

[40] Hesp, S.A.M., Low-Temperature Fracture in Asphalt Binders, Mastics, and Mixturesl In: Modeling of asphalt Concrete, Y. Richard Kim (Ed.), American Society for Civil Engineering, 15(2008)429-453.

[41] Howard, S.A. and Preston, K.D., Profile Fitting of Powder Diffraction Patterns, Reviews in Mineralogy vol 20: Modern Powder Diffraction, Mineralogical Society of America, Washington DC, 1989.

[42] Hussam, H.I., and Raphael, O.I., Interrelationships between Asphaltene Precipitation Inhibitor Effectiveness, Asphaltenes Characteristics, and Precipitation

Behavior during n-Heptane (Light Paraffin Hydrocarbon)-Induced Asphaltene Precipitation, Energy and Fuels, 18(2004)1038-1048.

[43] IP 143/84, Asphaltene Precipitation with Normal Heptane, Standard Methods for Analysis and Testing of Petroleum and Related Products, Institute of Petroleum, London, 1(1988).

[44] Jayaraj, C., Amarjeet, S.S., Gurpreet S.K., Agadi K., Babu R.T., Mukesh C.J., Surendra K.J. and Akhilesh K.B., Fuel, 75(1996)999-1008.

[45] Jen, T.E., Erdman, I.G. and Pollack, S.S., Investigation of the structure of petroleum asphaltenes by X-Ray Diffraction, Analytical Chemistry, 33(1961)1587.

[46] Jenkins, R., Snyder, R.L., Introduction to X-Ray Powder Diffractometry, John Wiley and Sons, Inc., New York, 1996.

[47] Keith L., Gawrys P., Matthew S. and Peter k.k., The Role of Asphaltene Solubility and Chemical Composition on Asphaltene Aggregation, Petroleum Science and Technology, 21(2003)461-489.

[48] Kim, Y.R., Modeling of Asphalt Concrete, MH/ASCE Press, First Edition, 2008.

[49] Klug, H.P. and Alexander, L.E., X-ray Diffraction Procedures, Second Edition, New York: John Wiley and Sons, (1974)618-708.

[50] Koots, J.A., and Speight, J.G., Relation of petroleum resins to asphaltenes, Fuel, 54(1975)179-184.

[51] Langford, J.I. and Wilson, A.J.C., Scherrer after Sixty Years: A Survey and Some New Results in the Determination of Crystallite Size, Journal of Applied Crystallography, 11(1978)102-113.

[52] Lee ,S., Amirkhanian, S.N., Park, N. Kim, K.W., Characterization of warm mix asphalt binders containing artificially long-term aged binders, Construction Building Materials 23(2009)2371-2379.

[53] LS-298, Asphalt Cement Grading for the Fracture Performance using Compact Tension Procedure, Ministry of Transportation of Ontario, Canada July 2005.

[54] Lu, X., Soenen, H. and Redelius, P., Impact of Bitumen Wax on Asphalt Performance-Low Temperature Cracking, Proceedings, 3rd Eurasphalt and Euro-bitume Congress, Vienna, May 12-14, 2004.

[55] Lu X., Redelius P., Composition and Structural Characterization of Waxes Isolated from Bitumen, Energy Fuels, 20(2006)653-66.

[56] Mansoori, G.A., Jiang, T.S., Kawanaka, S., Asphaltene Deposition and Its Role in Petrolum Production and Processing, Arab Journal of Science and engineering, 13(1988)17.

[57] McGennis, R.B., Anderson R.M., Kennedy T.W., Solaimanian, M., Background of Superpave Asphalt Mixture Design and Analysis, Publication No. FHWA-SA-95-003, (1994).

[58] Michael, G., Al-Siri, M., Khan, Z.H., and Ali, F.A., Differences in Average Chemical Structures of Asphaltene Fractions Separated From Feed and Product Oils of a Mild Thermal Processing reaction, Energy and Fuel, 19(2005)1598-1605.

[59] Mamlouk, M.S. and Zaniewski, J.P., Materials for Civil and Construction Engineers, Second Edition, Pearson Eduction, Inc., NJ, 2009.

[60] Monismith, C.J., Epps, J.A., Finn, F.N., Improved Asphalt Mix Design, Proceedings of the Association of Asphalt Paving Technologists, 54(1985)347-406.

[61] Moschopedis, S.E., Fryer, J.F. and Speight, J.G., Investigations of the carbonyl functions in a resin fraction from Athabasca bitumen, Fuel, 55(1976)184.

[62] Mullins O.C., The asphaltenes, Annu. Rev. Anal. Chem., 4(2011)(393-418).

[63] Mullins, O.C., The Modified Yen Model, Energy Fuels, 24(2010)2179-2207.

[64] Mullins, O.C., Andrews, A.B., Pomerantz, A.E., Dong, C., Zuo, J.Y., Pfeiffer, T., Latifzai, A.S., Elshahawi, H., Barr, L. and Larter, S.(2011), Impact of Asphaltene Nanoscience on Understanding Oilfield Reservoirs, Paper SPE 146649 presented at the SPE Annual Technical Conference and Exhibition, Denver, 30 October-2 November, 2011.

[65] Mullins, O.C., Hassan, O.S., Joelle E., Andrew E.P., Loic B., Andrews, A.B., Yosadara, R-M., Farshid M., Richard M., Lamia G.,Richard L., Thomas C., Jhony O., Roger M.L., John E., and Richard N.Z., Advances in Asphaltene Science and the Yen-Mullins Model, Energy and Fuel, (2012).

[66] Mullins, O.C., Sheu, E.Y., Hammami, A. and Marshall A.G., Asphaltenes, Heavy Oils and Petroleomics, Springer, NY, USA, 2007.

[67] Nikhil, B.J., Mullins, O.C., Jamaluddin, A., Creek, J. and McFadden, J., Asphaltene Precipitation from Live Crude Oil, Energy and Fuels, 15(2001)979-986.

[68] Narve, A., Harald, K., Einar, E.J. and Johan, S., Asphaltene Aggregation from Crude Oils and Model Systems Studied by High-Pressure NIR Spectroscopy, Energy and Fuels, 16(2002)1287-1295.

[69] Nellensteyn, F.J., World Petrolum Congress (3rd Ed.), 2(1933)616.

[70] Pecharsky, V.K. and Zavalij, P.Y., Foundamentals of Poweder Diffraction and Structural Charachterization of Materials, Springer, 2005.

[71] Peramanu, S., Singh, C., Agrawala, M. and Yarranton, H.W., Investigation on the Reversibility of Asphaltene Precipitation, Energy and Fuels, 15(2001)910-917.

[72] Philip, R.H., John E.P., and George F.A.B., Oxidation of Roading Asphalts, Znd. Eng. Chem. Res., 33(1994)2801-2809.

[73] Raveya, J.C., Ducouret, G., Espinat, D., Asphaltene macrostructure by small angle neutron scattering, Fuel, 67(1988)1560-1567.

[74] Richard, F., Ted S.V., Low-Temperature Cracking and Aging Performance of Modified Asphalt Concrete Specimens, Journal of the Transportation Research Board, 1998(2007)77-86.

[75] Roberts, F.L., Kandhal, P.S., Brown, R., Lee, D.Y., and Kennedy, T.W., Hot Mix Asphalt Materials, Mixture Design and Construction, First Edition, 1991.

[76] Roberts, F.L., Kandhal P.S., Brown, E.R., Lee D.Y., and Kennedy T.W., Hot Mix Asphalt Materials, Mixture Design, and Construction, National Asphalt Paving Association Education Foundation, Lanham, MD,1996.

[77] Sadeghi, M.A., Chilingarian, G.V. and Yen, T.F. American Chemical Society Syrup. Ser. 1986, g, 99 (Chem. Abstr. 104: 151905R).

[78] Sarowha, S.L.S. and Singh, I.D., Compositional and Structural Studies of Petroleum Asphaltenes Employing Spectroscopic Sechniques, Fuel, 67(1988)145.

[79] Scherrer, P., Bestimmung der Grsse und der inneren Struktur von Kolloidteilchen mittels Rntgenstrahlen, Nachr. Ges. Wiss. Gttingen, 26(1918)98-100.

[80] Schwager, I., Farmanian, P.A., Kwan, T.T., Weinburg, V.A. and Yen, T.F., Characterization of the Microstructure and Macrostructure of Coal-derived As-

phaltenes by Nuclear Magnetic Resonance Spectrometry and X-ray Diffraction, Analytical Chemistry, 55(1983)42.

[81] Schwartz, L.H. and Cohen, J.B., Diffraction from Materials, New York: Academic Press, (1977)391.

[82] Sergienko,S.R., High-Molecular-Weight Compounds of Crude Petroleum, Khimiya, Moscow, (1964).

[83] Shenkin, S.P., In 'Symposium on Average Structure Determination', Division of Petroleum Chemistry, American Chemical Society, Washington, DC, (1983)1367.

[84] Shenoy, A., Prediction of high temperature rheological properties of aged asphalts from the flow data of the original unaged samples, Construction and Building Materials, 16(2002)509-517.

[85] Sheu, E.Y., Petroleum Asphaltenes Properties, Characterization, and Issues, Energy and Fuels, 16(2002)74-82.

[86] Shirokoff, J.W., Siddiqui, M.N. and Ali, M.F., Characterization of the Structure of Saudi Crude Asphaltenes by X-ray Diffraction, Energy and Fuel, 11(1997)561-565.

[87] Shirokoff, J. and Lewis, J.C., Aromaticity Parameters in Asphalt Binders Calculated From Profile Fitting X-ray Line Spectra Using Pearson VII and Pseudo-Voigt Functions, 20th International Conference on Spectral Line Shapes, CP 1290, AIP (2010)274-278.

[88] Siddiqui, M.N., Ali, M.F. and Shirokoff, J., Use of X-ray Technique in Assessing The Aging Patterns of Asphalt Fractions, Fuel, 81(2002)51-58.

[89] Snape, C.E., Ladner, W.R. and Bartle, K.D., An Investigation of the oxygen and nitrogen groups In Super Critical Gas Extracts of Coal by n.m.r., Analytical Chemistry, 51(1979)2189.

[90] Snape, C.E. and March, M.K., In 'Symposium on Magnetic Resonance of Heavy Ends', Division of Petroleum Chemistry, American Chemical Society, Miami, 1985.

[91] Speight, J.G., The Chemistry and Technology of Petroleum, Fuel, 50(1971)102.

[92] Speight, J.G, The application of spectroscopic techniques to the structural analysis of coal and petroleum, Appl. Spec. Rev., 5(1972)211.

[93] Speight, J.G.,The Chemistry and Technology of Petroleum, 3rd Ed., New York: Marcel Decker Inc., 1999.

[94] Speight, J.G., Wernick, D.L., Gould, K.A. Overfield, R.E., Rao, B.M.L., Savage, D.W., Molecular Weight and Association of Asphaltenes: A Critical Review. Rev. Inst. Fr. Pet., 40(1985)51-61.

[95] Stastna, J., Zanzotto, L. and Vacin, O.J., Viscosity Function in Polymer-Modified Asphalts, Journal of Colloid Interface Sci., 259(2003)200-207.

[96] Strausz, P.O., Mojelsky, T.W. and Lown, E.M.,The Molecular Structure of Asphaltene: An unfolding Story, Fuel, 71(1992)1355.

[97] Suzuki, T., Itoh, M., Takegami, Y. and Watanabe, Y, Chemical structure of tarsand bitumens by 13C and 1H n.m.r. spectroscopic methods, Fuel, 61(1982)402.

[98] Tharanivasan, A.K., Svrcek, W.Y., and Yarranton, H.W., Measurement and Modeling of Asphaltene Precipitation from Crude Oil Blends, Energy and Fuels, 23(2009)3971-3980.

[99] Trejo, F., Ancheyta, J., Morgan, T.J., Herod, A.A., Kandiyoti, R., Characterization of asphaltenes from hydrotreated products by SEC, LDMS, LAMDI, NMR, and XRD, Energy and Fuels, 21(2007)2121-2128.

[100] WWW.asphaltmodelsetg.org/Pauli, Asphalt Research Consortium Asphalt Microstructure Modeling, 2010.

[101] WWW.eapa.org/asphalt, European Asphalt Pavement Association (EAPA), 2010.

[102] Wen, C.S., Chilingarian, G.V. and Yen, T.F., Properties and Structure of Bitumens, in Bitumens, Asphalts and Tar Sands, edited by G.V. Chilingarian, T.F. Yen, Developments in Petroleum Science 7, Elsevier Scientific Publishing Co., Amsterdam, 1978, Ch.7, pp. 155-190.

[103] Williams, R.B., In 'Symposium on Composition of Petroleum Oils Determination and Evaluation', ASTM Special Technical Publication, 224(1988)168.

[104] Wu, S., Cong, P., Yu, J. and Luo, X., Experimental Investigation of Related Properties of Asphalt Binders Containing Various Flame Retardants, Fuel, 85(2006)1298-1304.

[105] Xiaohu, L. and Ulf I., Effect of Aging on Bitumen Chemistry and Rheology, Construction and Building Materials, 16(2002)15-22.

[106] Xu, Y., Koga Y., Strausz, O.P., Characterization of Athabasca asphaltenes by small-angle x-ray scattering, Fuel, 74(1995)960-964.

[107] Yapp, M.T., Durrani, A.Z. and Finn, F.N., HP-GPC and Asphalt Characterization Literature Review, Report SHRP-A-503, Strategic Highway Research Program, National Research Council, Washington, D.C., 1991.

[108] Yasar M., Akınaz, S. and Gurkaynak, M.A. : Investigation of The Molecular Structure of Turkish Asphaltenes, Petroleum Science and Technology, 27:10(2009)1044-1061.

[109] Yen, T.F., Structure of Petroleum Asphaltene and Its Significance, Energy Sources, 1(1974)447.

[110] Yen, T.F., Chilingarian, G.V., Eds., Asphaltenes and Asphalts, Elsevier Scientific Publishing Co. : Amsterdam, The Netherlands, 2(2000).

[111] Yen, T.F., Erdman, G.J. Pollack, S.S., Investigation of The Structure of Petroleum Asphaltenes by X-ray Diffraction, Analytical Chemistry, 33(1961)1587-1594.

[112] Yen, T.F. and Erdman, J.G., In 'Encyclopedia of X-rays and Gamma Rays' (Ed. G.L. Clark), Reinhold, New York, (1963)65.

[113] Yu, J.Y., Feng, P.C., Zang, H.L., Wu, S.P., Effect of organo-montmorillonite on aging properties of asphalt, Construction and Building Materials, Article in press, 2009.

Appendices

6.1 Procedure for Profile Fitting a Diffraction Pattern

a. Open the diffraction pattern

b. Overlay the PDF reference

c. Zoom in on first peak(s) to analyze

d. Open the profile fitting dialogue to configure options

e. Refine the profile fit for the first peak(s)

f. Review the quality of profile fit

g. Move to next peak(s) and profile fit

h. Continue until entire pattern is fit

6.2 More simulations using XRD
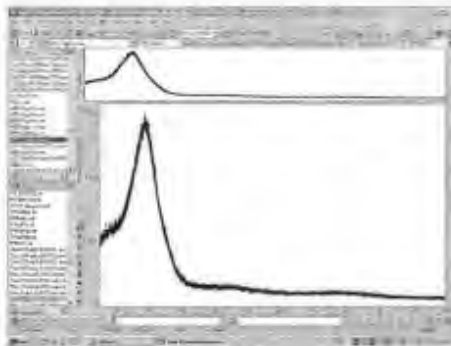
Figure 6.1: Specimen T1 on XRD
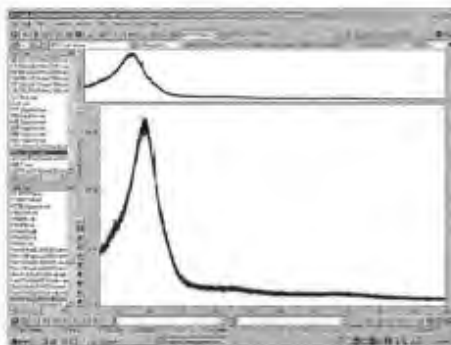
Figure 6.2: Specimen T2 on XRD
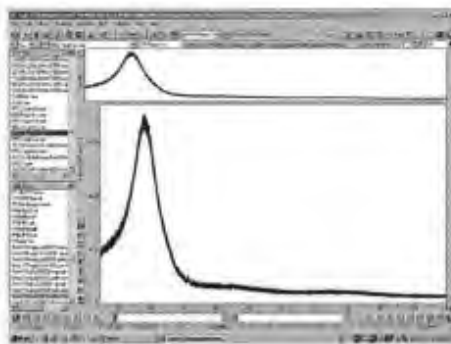
Figure 6.3: Specimen T3 on XRD
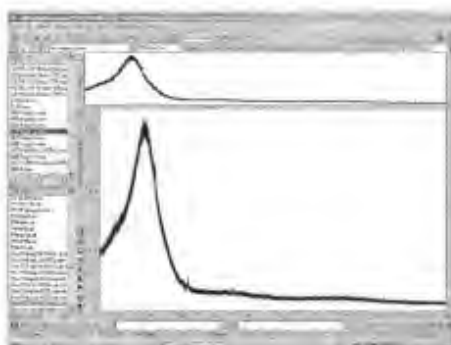
Figure 6.4: Specimen T4 on XRD
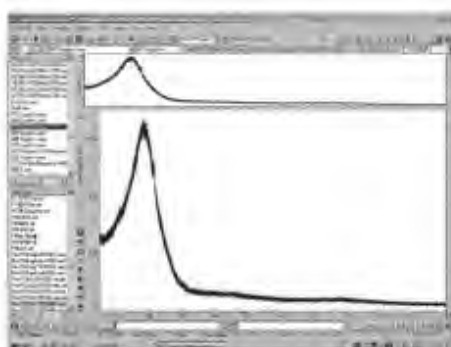
Figure 6.5: Specimen T5 on XRD
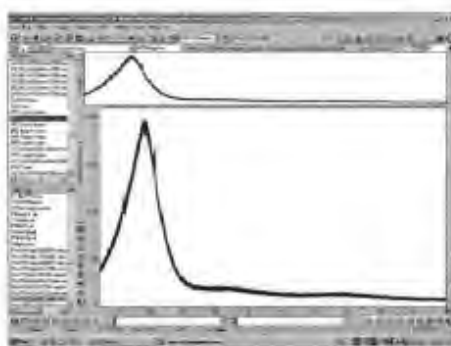
Figure 6.6: Specimen T6 on XRD
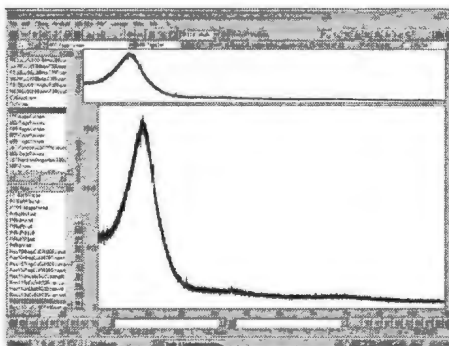
Figure 6.7: Specimen T7 on XRD
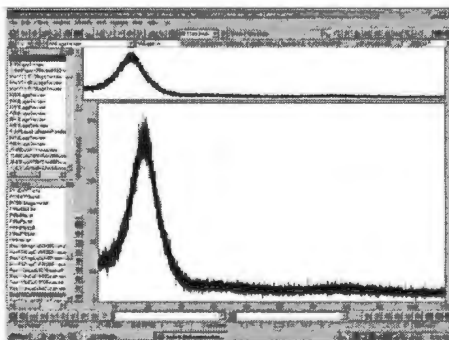
Figure 6.8: Specimen AAE on XRD

6.3 GFF routine using Mathematica

On the Generalised Fermi Function

```
Clear["Global`*"]
```

Assuming$\left[A > 0 \text{ \&\& } a > 0 \text{ \&\& } b > 0 \text{ \&\& } c > 0, \text{ Refine}\left[\int_{-\infty}^{\infty} A / \left(e^{-a(x-c)} + e^{b(x-c)}\right) dx\right]\right]$

$$A\left(\frac{e^{\ldots} \text{Hyp} \ldots}{a} + \frac{e^{\ldots} \text{Hyp} \ldots}{b}\right)$$

Numerical Integration

- An example:

$A = 322.37277900676656`; a = 0.0019370868376361658`; b = 0.5568927127875077`; c = 25.454496619627367`;$

```
NIntegrate[A/(Exp[-a(x-c)]+Exp[b(x-c)]),{x,0,15}]
```

8712.95

```
Clear["Global`*"]

dF = Length[dataFull]
10501

plotData =
 ListPlot[dataFull, PlotRange → {{10, 110}, {0, 2200}}, AxesOrigin→ {0, 0}, PlotStyle → {Thick, Blue},
  GridLines→ {{0, 5, 10, 15, 18.5, 20, 21, 25, 30, 35, 40, 44, 45, 50, 55, 60, 65,
     70, 75, 79, 80, 85, 90, 95, 100, 105, 110}, {0, 100, 200, 300, 400, 500, 600, 700,
     800, 900, 1000, 1100, 1200, 1300, 1400, 1500, 1600, 1700, 1800, 1900, 2000}}]


y2 =
 FindFit[dataFull, A1/ (E^(-a1 (s - c1)) + E^(b1 (s - c1))) + A2/ (E^(-a2 (s - c2)) + E^(b2 (s - c2))) + d,
  {{A1, 450.94417}, {a1, 0.24297}, {b1, 0.42078}, {c1, 30.0},
   {A2, 161}, {a2, 0.325}, {b2, 0.475}, {c2, 27.8}, {d, 30}}, s]

{A1 → 210.164, a1 → 0.981095, b1 → 0.0372906, c1 → 4.59825,
 A2 → 1846.84, a2 → 0.200005, b2 → 0.341408, c2 → 19.1755, d → 31.558}

fitData = Plot[
  ReplaceAll[A1/ (E^(-a1 (s - c1)) + E^(b1 (s - c1))) + A2/ (E^(-a2 (s - c2)) + E^(b2 (s - c2))) + d, y2],
  {s, 5, 110}, PlotRange → {{10, 110}, {0, 2200}},
  GridLines → {{0, 5, 10, 15, 18.5, 20, 21, 25, 30, 35, 40, 44, 45, 50, 55, 60, 65, 70, 75, 79,
     80, 85, 90, 95, 100, 105, 110}, {0, 100, 200, 300, 400, 500, 600, 700, 800, 900, 1000,
     1100, 1200, 1300, 1400, 1500, 1600, 1700, 1800, 1900, 2000}}, PlotStyle → {Thick, Red}]


Show[plotData, fitData]


plotData = ListPlot[dataFull, PlotRange → {{10, 110}, {0, 2200}},
  GridLines → {{0, 5, 10, 15, 18.5, 20, 21, 25, 30, 35, 40, 44, 45, 50, 55, 60, 65, 70, 75, 79, 80, 85, 90,
     95, 100, 105, 110}, {0, 100, 200, 300, 400, 500, 600, 700, 800, 900, 1000, 1100, 1200, 1300,
     1400, 1500, 1600, 1700, 1800, 1900, 2000}}, AxesOrigin → {0, 0}, PlotStyle → {Thick, Brown}]


y2 = FindFit[dataFull,
  A1/ (E^(-a1 (s - c1)) + E^(b1 (s - c1))) + A2/ (E^(-a2 (s - c2)) + E^(b2 (s - c2))) + da + db s,
  {{A1, 1611.11}, {a1, .244154}, {b1, 0.569322}, {c1, 30.0}, {A2, 3375},
   {a2, 0.0325}, {b2, 0.422051}, {c2, 27.8}, {da, 195}, {db, -1}}, s]

{A1 → 232.815, a1 → 1.0661, b1 → 0.208908, c1 → 23.3445, A2 → 1761.04,
 a2 → 0.140826, b2 → 0.499858, c2 → 20.1715, da → 116.657, db → -0.827435}

fitData = Plot[ReplaceAll[
  A1/ (E^(-a1 (s - c1)) + E^(b1 (s - c1))) + A2/ (E^(-a2 (s - c2)) + E^(b2 (s - c2))) + da + db s, y2],
  {s, 5, 110}, PlotRange → {{10, 110}, {0, 2000}},
  GridLines → {{0, 5, 10, 15, 18.5, 20, 21, 25, 30, 35, 40, 44, 45, 50, 55, 60, 65, 70, 75, 79,
     80, 85, 90, 95, 100, 105, 110}, {0, 100, 200, 300, 400, 500, 600, 700, 800, 900, 1000,
     1100, 1200, 1300, 1400, 1500, 1600, 1700, 1800, 1900, 2000}}, PlotStyle → {Thick, Red}]
```

.

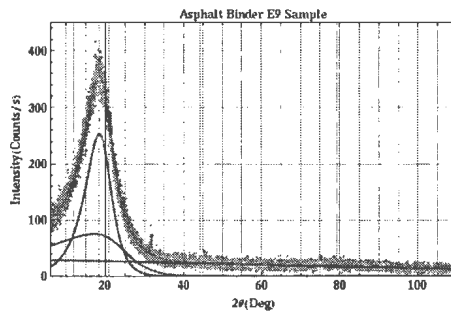## 6.4 More simulations using Mathematica for fitting the samples with GFF
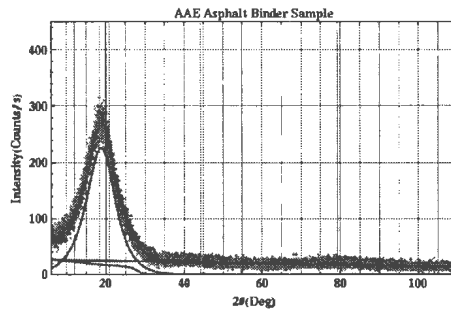

Figure 6.9: Specimen E9 on GFF
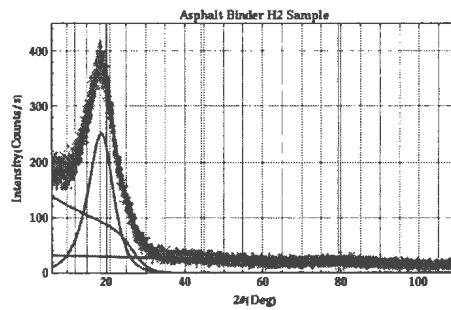

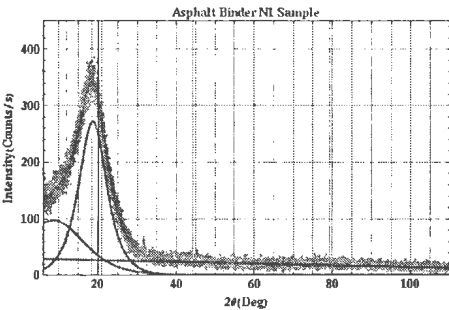Figure 6.10: Specimen AAE on GFF

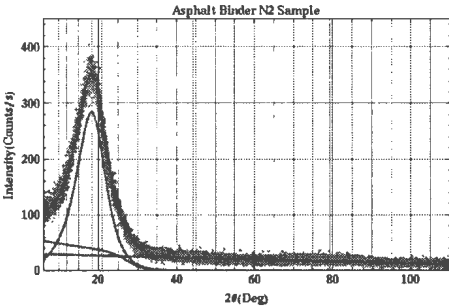Figure 6.11: Specimen H2 on GFF

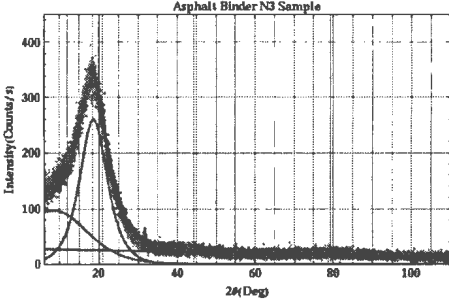Figure 6.12: Specimen N1 on GFF

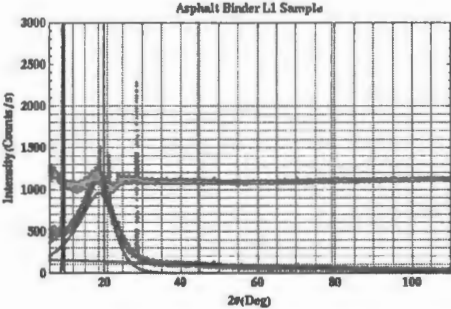Figure 6.13: Specimen N2 on GFF

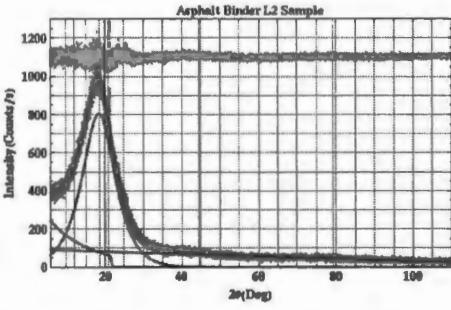Figure 6.14: Specimen N3 on GFF

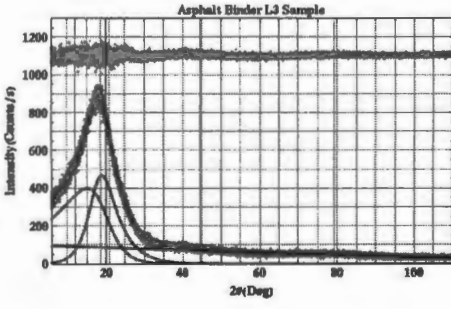Figure 6.15: Specimen L1 on GFF

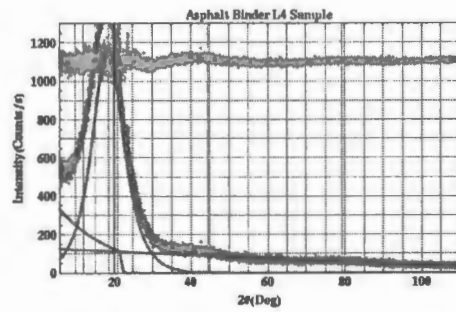Figure 6.16: Specimen L2 on GFF

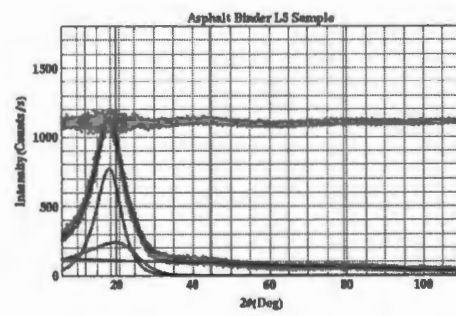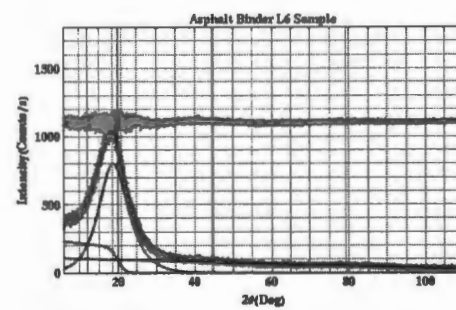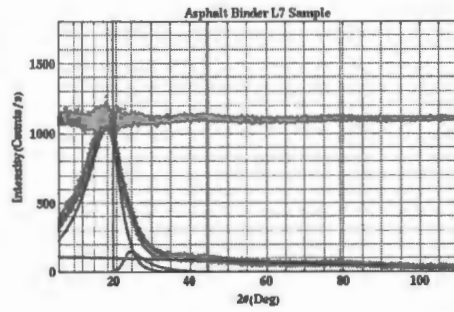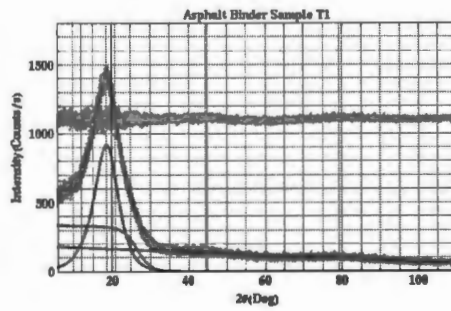Figure 6.17: Specimen L3 on GFF

Figure 6.18: Specimen L4 on GFF

Figure 6.19: Specimen L5 on GFF

Figure 6.20: Specimen L6 on GFF

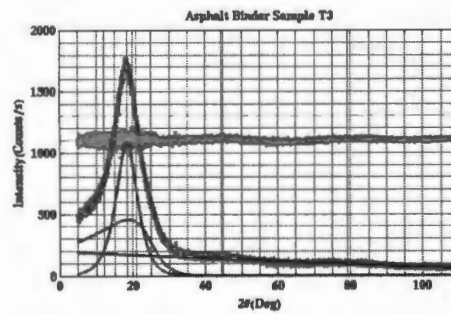Figure 6.21: Specimen L7 on GFF

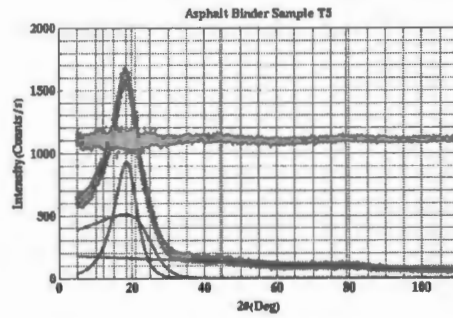Figure 6.22: Specimen T1 on GFF

Figure 6.23: Specimen T3 on GFF
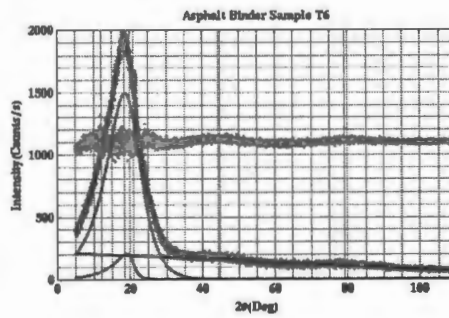
Figure 6.24: Specimen T5 on GFF

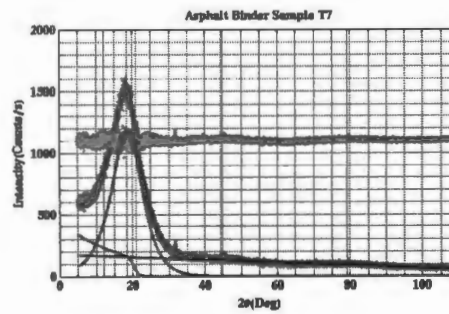Figure 6.25: Specimen T6 on GFF

Figure 6.26: Specimen T7 on GFF

6.5   Procedure to follow Gaussian and Lorentzian analysis

In the final procedure, the following steps are employed:

(i) select a background at the lowest value in the range $2\theta = 70°$.

(ii) fit the (100) band while giving initial values to other peaks.

(iii) fit the γ peak and the (002) peak with initial estimates that aim at reproducing the shape of the summed peak.

(iv) manually optimize the peak position and width while regressing the peak.

(v) finally perform a regression analysis of each individual peak position. This procedure does not include consideration of the minimum region between the (002) peak and the (100) peak that, in some Gaussian cases, required an additional peak at 2θ 30° that has not been assigned to any crystallite component.